Journal of Structural Geology 31 (2009) 691–706

Contents lists available at ScienceDirect

Journal of Structural Geology

journal homepage: www.elsevier.com/locate/jsg

Kinematic vorticity flow analysis and $^{40}Ar/^{39}Ar$ geochronology related to inclined extrusion of the HP–LT metamorphic rocks along the Zagros accretionary prism, Iran

Khalil Sarkarinejad [a,*], Laurent Godin [b], Ali Faghih [a]

[a] Department of Earth Sciences, College of Sciences, Shiraz University, Shiraz 71454, Fars Iran
[b] Department of Geological Sciences and Geological Engineering, Miller Hall, Queen's University, Kingston, Ontario K7L3 NG, Canada

ARTICLE INFO

Article history:
Received 14 July 2008
Received in revised form
18 March 2009
Accepted 12 April 2009
Available online 18 April 2009

Keywords:
Zagros accretionary prism
Zagros thrust system
Melange
Kinematic vorticity number
Iran

ABSTRACT

The Zagros accretionary prism in southwestern Iran is exposed along the NW–SE trending of the Zagros Thrust System and inclined Zagros transpression zone. This accretionary prism consists of two units: the upper sedimentary mélange unit on top and the high-pressure metamorphic mélange unit at the bottom. Both units show characteristics of a tectonic wedge. The upper unit consists of type-I, II and III mélanges which display S-, C- and C′-type shear-band cleavages, quartz ribbons and rectangular or fish-head boudins. The lower unit fabrics display σ-, and δ-type porphyroclasts and quartz ribbon mylonites. These fabrics formed from a combination of 60.5% simple shear and 39.5% pure shear. Both components were involved in a lateral exhumation of the high-pressure/low-temperature metamorphic rocks in an inclined transpression wedge-shaped geometry. The estimated kinematic vorticity number (W_k) was calculated from quartz c-axis patterns, rotation of porphyroclasts and orientation of finite strain with respect to shear zone boundaries. Using the mean estimated W_m value of 0.84, the inclination angle for the thrust wedge on top of the NE-subducting Neo-Tethyan oceanic lithosphere is 18°. The $^{40}Ar/^{39}Ar$ plateau ages of early generations of biotite from the lower metamorphic mélange are 119.95 ± 0.88 Ma and 112.58 ± 0.66 Ma. This late Aptian age is related to early thrusting and formation of HP–LT metamorphic rocks. The dating of two amphibole samples from the amphibolite yields a weighted mean age of 91.23 ± 0.89 Ma. This Turonian–Cenomanian age suggests a later metamorphic event associated with subduction and obduction of the Neyriz ophiolite and later lateral extrusion of HP–LT metamorphic rocks along the inclined Zagros accretionary prism.
© 2009 Elsevier Ltd. All rights reserved.

1. Introduction

Most accretionary prisms form wedge-shaped structures bounded by a roof thrust along their upper surface and a floor thrust beneath (Chi et al., 2003. In such wedge-shaped structures the convergence direction is oblique or inclined, and the zone boundaries are non-planar (Jones et al., 2004; Sarkarinejad, 2007; Sarkarinejad and Azizi, 2008). During oblique or inclined transpression, there is tendency for pure-shear and simple-shear strain components to occur in spatially separated domains (Fossen et al., 1994; Tikoff and Teyssier, 1994; Teyssier et al., 1995; Jones and Tanner, 1995). Fossen and Tikoff (1993) divided transpression into pure-shear dominated and simple-shear dominated, depending on the angle of convergence as defined by infinitesimal strain axes. These two cases can be differentiated using the kinematic vorticity number W_k (Fossen and Tikoff, 1993), which is a non-linear ratio of the pure-shear to simple-shear component (Tikoff and Teyssier, 1994). There is an angular relationship θ between the maximum horizontal axis of the instantaneous strain ellipsoid and the boundary zones (Fossen and Tikoff, 1993). The angle θ is also related to α, the angle of oblique plate convergence or flow apophysis (Tikoff and Teyssier, 1994). Based on theoretical modeling, Fossen and Tikoff (1993) suggested that simple-shear dominated transpression occurs when $1 > W_k > 0.81$ and $35° < \theta < 45°$ whereas pure-shear dominated transpression occurs when $0.81 > W_k > 0$ and $0° < \theta < 35°$.

Strain matrix modeling of transpressional deformation shows that all three axes of the finite strain ellipsoid are non-parallel to the Cartesian reference frame which experiences complex non-planar rotations during ongoing deformation (Jones et al., 2004). The maximum finite strain axis and material lines are always "attracted" to the extensional flow apophysis (or maximum extensional flow direction) (Fossen et al., 1994; Passchier, 1997).

* Corresponding author. Tel.: +98 711 8321348; fax: +98 711 2284572.
E-mail addresses: sarkarinejad@geology.susc.ac.ir (K. Sarkarinejad), godin@geol.queensu.ca (L. Godin), afaghih@shirazu.ac.ir (A. Faghih).

0191-8141/$ – see front matter © 2009 Elsevier Ltd. All rights reserved.
doi:10.1016/j.jsg.2009.04.003

Consequently, a relation exists between the orientation of strain/fabric and principal flow directions (Teyssier and Tikoff, 1999). Theoretical modeling predicts that the maximum finite strain axis or stretching lineation switches from horizontal to vertical with increasing strain (monoclinic transpression; Sanderson and Marchini, 1984) or when the stretching lineation lies almost strike-parallel or is significantly oblique or approximately down dip (triclinic transpression; Jones and Holdsworth, 1998; Jones et al., 2004). In all of these models, idealized boundary conditions are assumed, as defined by Sanderson and Marchini: deformation is homogeneous, constant volume, laterally and basally confined, and occurs between parallel zone boundaries (Jones et al., 2004).

Accretionary prisms form marginal boundary zones in which the deeply subducted and "transpressed" rocks act as viscous materials squeezed between two inclined rigid plates. This paper describes structures and microstructures related to real transpressional zones to test the applicability of the simplified stain matrix modeling. The objectives of this paper are: (1) to describe the dominant fabrics identified in the upper sedimentary and lower metamorphic mélanges, (2) to investigate the *c*-axis preferred orientations from quartz ribbons, (3) to estimate the kinematic vorticity number for quantifying pure-shear and simple-shear components, (4) to use geochronology to obtain absolute ages for the deformation events.

2. Geology of the Neyriz area

The Neyriz area is located in southwestern Iran. This area has an excellent exposure of the Neyriz ophiolite, the Zagros thrust system, the Hassan Abad upper sedimentary tectonic mélange, the Seh-Ghalatoun lower metamorphic tectonic mélange and the HP–LT/HT–LP Sanandaj-Sirjan paired metamorphic belts (Fig. 1). The Zagros orogenic belt is the central part of the Alpine–Himalayan mountain chain. This orogenic belt extends for more than 2000 km in a NW–SE direction from eastern Turkey to the Minab-Zendan fault system in southern Iran (Haynes and McQuillan, 1974; Stocklin, 1974. This belt resulted from the closure of the Neo-Tethyan Ocean due to northeast-dipping subduction below the Iranian microcontinent (Alavi, 1994; Vernant et al., 2004).

The geodynamics of the region are dominated by the convergence between the Arabian and Eurasian plates (Jackson and Mckenzie, 1984). Compressional structures related to the closure of the Neo-Tethyan Ocean (e.g. Stocklin, 1968; Falcon, 1974; Berberian and King, 1981; Alavi, 1994) strike oblique to the convergence direction. This obliquity is probably due to the pure-shear dominated transpression and shortening accommodated by imbricate thrusting as well as oblique extrusion of deeply subducted high-grade metamorphic rocks (Sarkarinejad, 2003, 2005, 2007; Sarkarinejad and Azizi, 2008).

2.1. Structure of the Neyriz ophiolite

The Neyriz ophiolite (Fig. 1), exposed in the southwestern part of the Sanandaj-Sirjan metamorphic belts, is considered to consist of allochthonous fragments of the Tethyan Oceanic crust and mantle (Gansser, 1974; Stocklin, 1968). The Neyriz ophiolite has been thrust over the Pichkun formation, consisting of abyssal sedimentary facies containing radiolarian cherts, fossiliferous limestone, turbidite, middle Jurassic oolitic and micro-brecciated limestone, and middle Cretaceous limestone (Ricou, 1968).

The Neyriz ophiolite is probably the largest, best exposed, and best-preserved example of oceanic lithosphere in Iran (Sarkarinejad, 2005). It includes the entire thickness of the deformed mantle section, from the ultramafic Moho Transition Zone (MTZ), to the mafic section which includes gabbros, sheeted dikes and pillow lavas, and to radiolarian cherts on top. The deformed mantle section (6 km thick) mostly consists of harzburgite, serpentinized harzburgite and lherzolite. In thin section the harzburgite shows coarse- to medium-grained porphyroclastic fabrics (Sarkarinejad, 2005). High-temperature (HT) deformation of the coarse-grained granoblastic structures is related to hypersolidus or solidus temperatures (1200°–1250 °C), and thus to large-scale plastic flow below the oceanic ridge. Medium-temperature (MT; 1100 °C) deformation is related to localized motion along shear zones and detachment thrusts (Nicolas et al., 2000). Construction of mantle flow trajectories based on detailed structural mapping of the Neyriz mantle section reveals three mantle diapirs aligned along the NW–SE direction (Sarkarinejad, 2005). They are characterized by steep foliations in the high-temperature harzburgite and an associated steeply dipping stretching lineation, reflecting localized vertical flow related to mantle diapirs (Sarkarinejad, 2005).

The Moho Transition Zone (MTZ) is composed of dunite, chromite clinopyroxenite and websterite. The clinopyroxene, orthopyroxene and olivine minerals of the MTZ are moderately deformed. Low-level layered gabbros are exposed on top of the MTZ. The normal sequence of the sheeted dikes, pillow lavas, overlying lava flows and radiolarian cherts is best exposed in the central part of the ophiolite sequence (Sarkarinejad, 2005). The sheeted dike complex is uniformly steep, inclined 66°–89° with a mean dip direction N 47° W, 67° NE (Sarkarinejad, 2005). The average orientation of the sheeted dikes is vertical and parallel to the paleo-ridge axis (Nicolas, 1989).

3. Mélange

The mélange outcrop is located in the east to northeastern part of the Neyriz ophiolite and extends along the Zagros thrust system (Fig. 1). The mélange is divided into two units based upon: (1) the lithology and origin of the blocks and surrounding matrix; (2) intensity of deformation and degree of metamorphism; (3) number of phases of deformation.

The upper Hassan Abad sedimentary mélange (Fig. 1) is exposed as a narrow shear zone along the Zagros thrust system. The mélange length extends approximately 53 km and its width varies from 250 to 3750 m. Excellent exposures of mélange are preserved in the road cuts along the Hassan Abad and Naghare-Khaneh passes. The mélange consists of lenses, blocks and/or ribbons of radiolarian cherts, limestone, sandstone, pillow lava, tuff, and serpentinite, in a matrix of shale, greywacke and mudstone (Sarkarinejad, 2003). The mélange lenses or blocks range in size from millimeters to several hundred meters. The sedimentary mélanges can be classified according to their fabrics; they include type-I, type-II and type-III tectonic mélanges.

3.1. Type-I mylonite mélange

The upper sedimentary mélange unit is a type-I mylonitic mélange. Three types of shear-band cleavages were distinguished in this mélange; C-type C′-type and S-type shear-band cleavages (Fig. 2A) corresponding to the C- and S-bands of Berthe et al. (1979a,b). The C-type is an extensional cleavage and is part of an S/C fabric that consists of S-planes transected by distinct planar C-type shear bands or C′-planes (Berthe et al., 1979a,b; Lister and Snoke, 1984). The angle between the C- and S-planes is 35°. The angle between the C- and C′-planes is 45°.

On the microscopic and mesoscopic-scales, porphyroclasts consist of fragments of sandstone, limestone, pillow lavas and

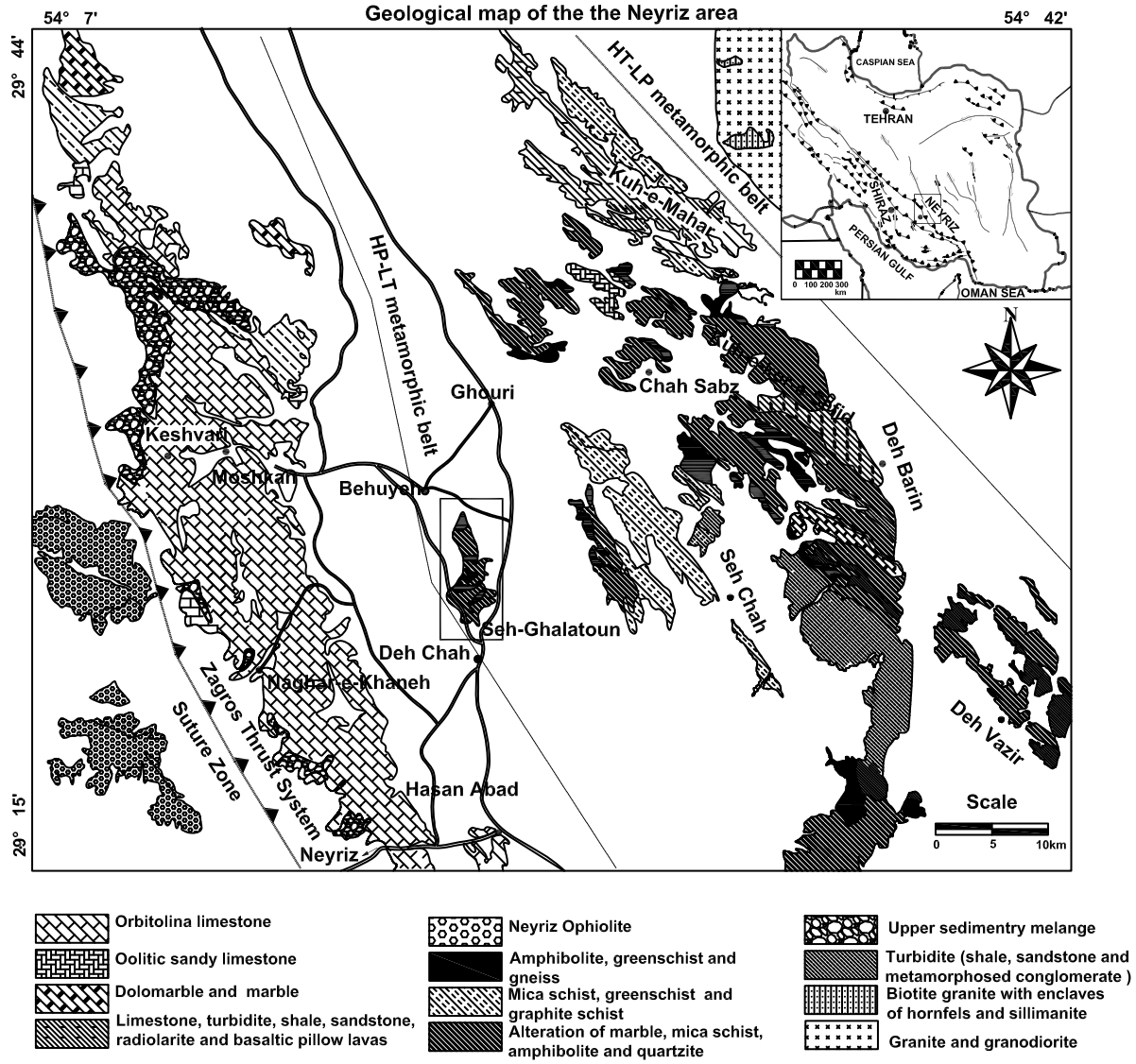

Fig. 1. Geological map of the Neyriz area showing the distribution of the upper sedimentary mélange along the Zagros thrust system. The rectangle in the southwestern part of the map is the Seh-Ghalatoun study area (Fig. 3) which lies in the western marginal part of the Sanandaj-Sirjan HP–LT metamorphic belt. This modified map is part of the 1:250,000 Neyriz quadrangle map from Sabzehei et al. (1993).

radiolarian chert. The matrix is mostly composed of fine-grained shale, marl, and greywacke. Both σ-type (symmetric) and δ-type (asymmetric) porphyroclasts are present (Fig. 2B; Passchier and Trouw, 2005). These porphyroclasts together with tectonic fish and foliation fish (Stock, 1992) in sections normal to the foliation plane and parallel to the stretching lineation were used as shear sense indicators. They all indicate a dextral sense of shear for the Zagros thrust system.

3.2. Type-II mélange

Type-II mélange is characterized by the presence of elongate clasts of fine-grained greywacke and limestone which are set in a matrix of mudstone or shale. The clasts form ribbons, stripes, rods or flattened lenses. Type-II mélange has a set of shear bands without clear S-planes (Lister and Snoke, 1984). The outcrop-scale fabrics typically vary in size from 5 to 60 cm in length. They mostly have a horizontal to sub-horizontal plunge and it is difficult to use them as shear sense indicators.

3.3. Type-III mélange

In the Type-III mélanges, stretched and relatively incompetent to competent rocks such as sandstone, radiolarian cherts, tuffs and limestone are present as boudins, ranging from rectangular to fish-head to barrel-shaped or pinch-and-swell (Fig. 2C). These boudins are set in a matrix of shale or mudstone. Most of the rectangular or barrel-shaped boudins are sub-parallel to the C-plane, whereas pinch-and-swell boudins are sub-parallel to the S-plane. The preferred orientation of elongated and rotated lens-shaped fragments defines a foliation (fragment foliation) that is sub-parallel to sedimentary layering on a large scale.

3.4. Lower HP–LT metamorphic mélange

The Seh-Ghalatoun *lower HP–LT* metamorphic mélange crops out near the village of Deh Chah, in the eastern part of the Neyriz ophiolite (Fig. 3). The predominant rocks in the area are amphibolite, garnet amphibolite, quartzo-feldspathic gneiss, kyanite

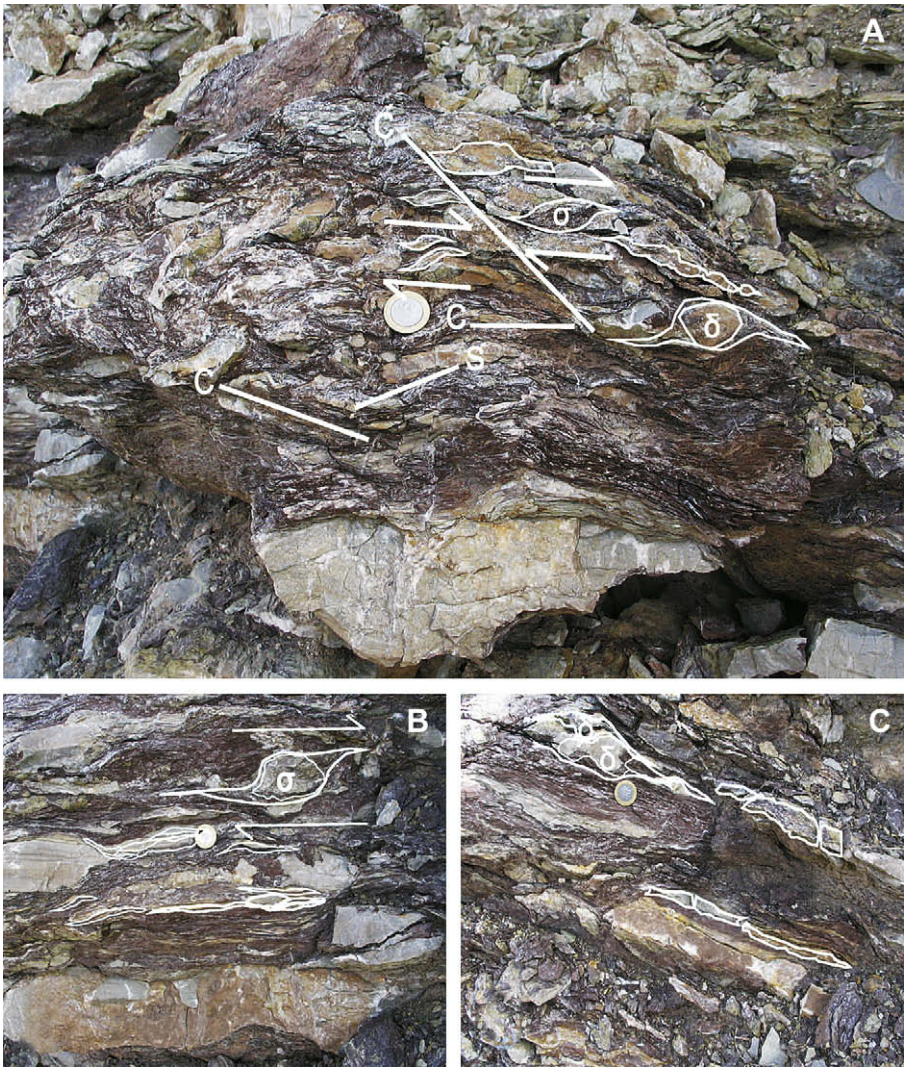

Fig. 2. (A) Upper sedimentary mélange showing type-I mylonite mélange with S/C shear-band cleavages, symmetrical σ-type and asymmetrical δ-type porphyroclasts and tectonic fish. (B) Type-II mélange characterized by the presence of elongated fine-grained greywacke and limestone forming ribbons, stripes, rods or flattened lenses. (C) Type-III mélange which includes pinch-and-swell, fish-head and barrel-shaped boudins.

gniess, biotite gneiss, muscovite-garnet schist and phyllite. The amphibolite and quartzo-feldspathic gneiss contain numerous continuous to discontinuous intercalations of eclogite facies rocks. These rocks, forming torn-, drawn-, and shear-band boudins, have a mineral assemblage of omphacite + pyrope-rich garnet + corundum + zircon + kyanite. Pink garnet is rimmed with deep green amphibole and abundant colorless omphacite. The eclogite facies is divided into two types: type I is coarse grained and type II is medium grained, based on the size of porphyroblastic pyrope-rich garnet. The mean size of type-I garnet is 10.26 ± 2.8 mm and that of type-II garnet is 5.8 ± 1.50 mm, and the mean size of omphacite grains is 0.82 ± 0.48 mm.

3.5. Blueschist facies

Blueschist facies rocks are not present in the Seh-Ghalatoun area, although some outcrop 12 km west of Neyriz. The blueschist facies slice is about 7 m long and 5 m wide in the olistostrome outcrop, and is associated with thick and thinly layered asymmetrically folded marble, amphibolite, serpentinized harzburgite and gabbros. The mineral assemblage of the strongly foliated and lineated blueschist facies is glaucophone + lowsonite + cordiorite + zeosite + chlorite + actinolite.

4. Deformation history of the metamorphic mélange

Three fabric-forming deformation phases were identified within the Seh-Ghalatoun area. Two fabrics are associated with the high-pressure/low-temperature metamorphism. Sarkarinejad (1999) suggested that the high-pressure rocks, which show characteristics of Alpine-type HP–LT metamorphism, are associated with the metamorphism of the Neyriz ophiolite slices. The third fabric was developed during deformation within shear zones.

5. Structures

5.1. Foliation (S_1)

The first generation of foliation (S_1) within the Seh-Ghalatoun area is a penetrative regional-scale foliation in the biotite gneiss, muscovite-garnet schist (Fig. 4A) and biotite schist. It is defined by the alignment of medium to coarse-grained muscovite and biotite

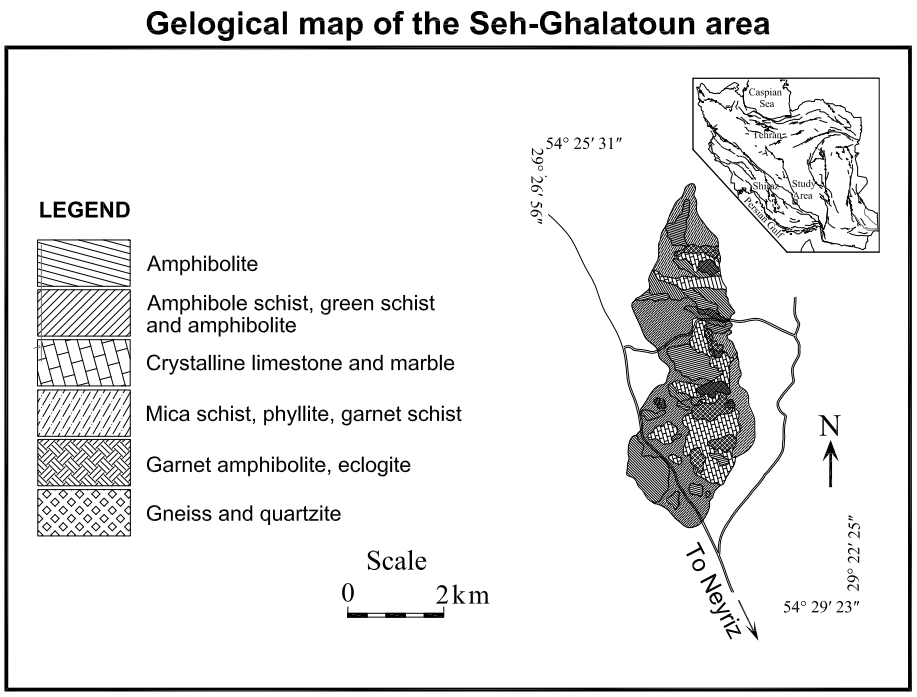

Fig. 3. Geological map of the Seh-Ghalatoun area showing major distribution of the high-pressure/low-temperature metamorphic rocks.

and elongated quartz grains. This foliation is oriented N 54° W, 58° NE, although it is highly variable with respect to the later folding.

5.2. Foliation (S_2)

The second generation of foliation (S_2) is a crenulation cleavage associated with differentiated garnet-muscovite schist, quartzo-feldspathic gneiss, and quartzite boudins within the biotite gneiss, and commonly lies at a high angle to S_1. The S_2 orientation is N 16° E, 81° W. The formation of this cleavage is due to asymmetrical chevron micro-folding of the S_1 foliation during D_2 deformation (Fig. 5A). The schist contains garnet porphyroblasts up to 3 cm in diameter and biotite grains up to 1 cm in length. In many areas several overprinting foliations can be recognized: a "main foliation" may have formed at the peak metamorphic conditions, whereas later deformation under lower grade conditions produced weaker or less penetrative foliations.

5.3. Lineation

The regional high-pressure metamorphic rocks have a well-developed mineral stretching lineation. During the development of the foliations, amphibole in the amphibolite, garnet amphibolite, gneiss, and greenschist developed a stretching lineation (Fig. 4B). The amphibolite and greenschist have been broken up into blocks and enclosed within the ductility sheared biotite gneiss, forming the lower metamorphic mélange. Most blocks are mechanically rotated and thus the lineation has a variable orientation.

The first generation and dominant mineral stretching lineation in the amphibolite and garnet amphibolite facies rocks is L_1 and it is generally associated with the S_1 foliation. The plunge and trend of L_1 averages 25°, S 3° E (Fig. 4B). A second lineation L_2 can be seen, with a plunge and trend varying from 36°, N 11° E to 36°, N 59° E. It is not clear, however, whether L_2 developed by mechanical rotation of L_1 or grew independently during D_2.

There are many varieties of boudins within the quartzo-feldspathic gneiss and amphibolites (Fig. 5B and C). The geometry of the boudins can be classified according to Goscombe and Passchier (2003) and Goscombe et al. (2004). The asymmetric types include domino boudins and shear-band boudins (Fig. 5B). The symmetric types include drawn boudins, pinch-and-swell structures and tapering boudins. Many boudins show polyphase deformation, and most are sheared, rotated, folded, and refolded. Domino boudins are either parallel or oblique to the S_1 foliation (Sarkarinejad, 2007).

The quartzite boudins were subjected to two phases of deformation. Quartzite layers were extended and boudinaged and then folded (Fig. 5D). F_1 folds are recumbent, isoclinal to moderately inclined, and asymmetric ($\phi \approx 130°$; ϕ is the bisector of folding angle). The mean axial trend of F_1 folded boudins within the area is N 77° W; the plunge varies from gentle (0°–15°) to moderately inclined (30°–60°) to the NE. The recumbent folds have been overprinted by second generation folds (F_2), producing type 3 interference patterns characterized by an undulating axial trace of F_1 (Ramsay, 1962; Ramsay and Huber, 1987). The F_2 folds are tight or isoclinal, with an axial trace that plunges shallowly (17°–32°) to moderately (34°–38°) to the NE.

6. Shear zones

The shear zone outcrops in the Seh-Ghalatoun and east of the Ghouri area are associated with the regional-scale Zagros thrust system and exhumation of deep-seated, high-grade metamorphic rocks such as amphibolite, garnet amphibolite, eclogite, and quartzo-feldspathic gneiss. Quartzite within these shear zones displays a variety of shapes. Most of the eye-shaped lenses, rods, flattened and rotated lenses, or extensional boudins of quartzite are surrounded by a matrix of biotite, feldspar, and quartz. They exhibit a well-defined S/C geometry over an area of 4–50 cm (Fig. 5C and D). The eye-shaped and sigmoidal-shaped quartzite boudins display winged σ- and δ-type porphyroclasts. Mantled porphyroclasts generally have wings with a gently curved centerline and

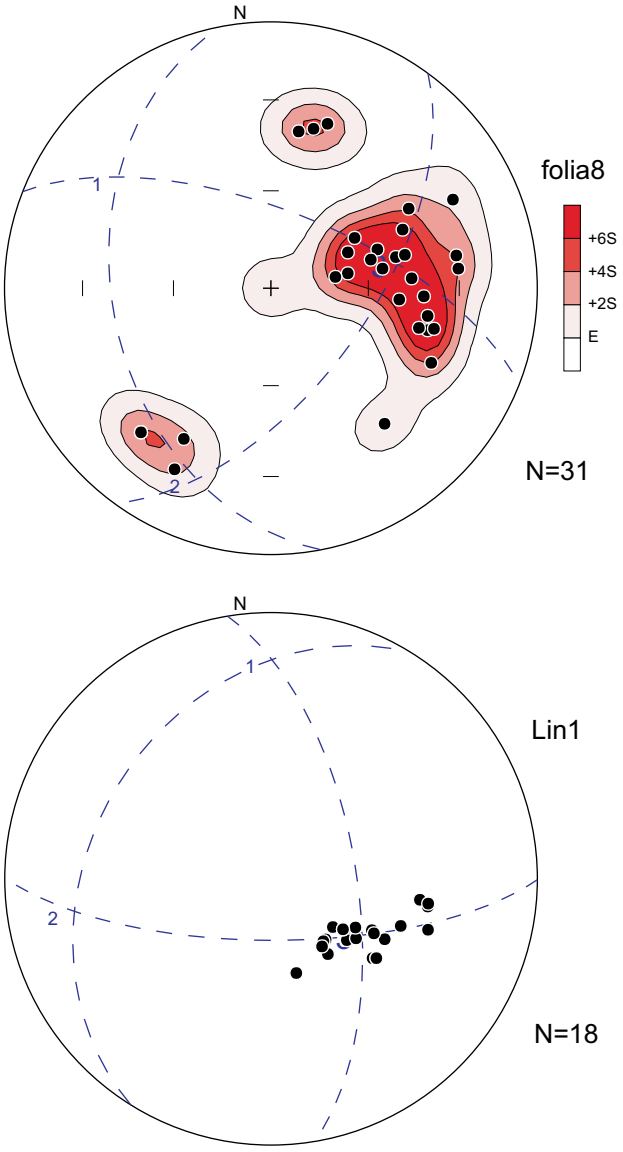

Fig. 4. Equal-area, lower hemisphere projections presenting data for poles for the Seh-Ghalatoun mica schist foliation. Dotted great circles 1, 2 and 3 represent the computed average v_1, v_2 and v_3 (eigenvectors). (A) Contours 2, 4 and 6% of the mica schist foliations (S_1). (B) Seh-Ghalatoun amphibole stretching lineation.

are symmetrical to asymmetrical. The δ-type porphyroclasts have strongly curved wings that are asymmetric. These porphyoclasts indicate a dextral sense of shear.

7. Microstructural analysis

7.1. Microstructures in the muscovite schist

Oriented samples of muscovite-garnet schist display differentiated crenulation cleavage or zonal asymmetrical cleavages (Fig. 6A). They show two domain structures with alternating intensity cleavage. Domain structures consist of alternating mica-rich domains (M) and microlithon domains with light-colored, coarser-grained zones of crenulated laminae of quartz. The S_1 and S_2 foliations (related to D_1 and D_2) commonly lie at an angle of 30°–50° to each other and are well preserved; the S_1 foliation trends NW–SE while S_2 is a differentiated cleavage trending NE–SW. S_1 and S_2 form asymmetrical micro-folds.

7.2. Microstructures of kyanite gneiss

Kyanite gneiss consists of kyanite, feldspar, biotite and quartz. The gneiss contains porphyroclasts of kyanite (1–5 cm in diameter) surrounded by feldspar, quartz, and biotite. Kyanite lies within the main foliation and forms micro-boudins (Fig. 6B). The micro-boudin necks or inter-boudin surfaces are composed of very fine-grained secondary minerals. The kyanite micro-boudins include symmetric drawn boudins and asymmetric domino boudins. The drawn boudins are symmetric with no block rotation, and layer extension was accommodated by differential stretch of both layer and host (Goscambe et al., 2004). The asymmetrical domino boudins with inter-boudin vein material superficially resemble simple dilatational domino boudins.

7.3. Microstructures of quartz ribbons

Microstructural analysis was carried out on oriented thin sections normal to the foliation plane and parallel to the stretching lineation (*XZ*-plane). The sections were cut from quartzite boudins within high-grade gneisses of the Seh-Ghalatoun and quartzite mylonites in the northeastern part of the Ghouri shear zones. They are composed of quartz ribbons and dynamically recrystallized quartz grains. The quartz ribbons commonly show undulatory extinction, deformation lamellae, sub-grains, and new grains (Fig. 6C and D). They have serrated straight and curved boundaries with a well-developed lattice preferred orientation (LPO). Coarse ribbon grains are common and have elongated shapes 0.2–40 mm long and 0.01–0.5 mm wide, with a mean aspect ratio of 12.5 ± 7.7.

Single rotated amphibole grains within a matrix of sigmodial quartz ribbons form mantled porphyroclasts (Fig. 6E). The quartz ribbons are deformed into wings that extend on both sides of the porphyroclast, parallel to the mylonitic fabric (Passchier and Simpson, 1986). These are δ-type porphyroclasts (Fig. 6E), which can be used as shear sense indicators. The internal asymmetry and the stair stepping of the quartz ribbon wings indicate dextral shear sense.

7.4. Quartz c-axis fabrics

Oriented samples from quartzite mylonites within the Seh-Ghalatoun gneisses and from the northeastern part of the Ghouri shear zones were selected for *c*-axis measurements using a 5-axis U-stage. Samples qaxes1 to qaxes4 come from the Seh-Ghalatoun outcrop and samples SZ-1, SZ-2, SZQ-1 to SZQ-6 come from the Ghouri shear zones. Measurements were carried out on thin sections cut in the *XZ*-plane of finite strain ellipsoid. The *c*-axis orientations were plotted with respect to the mesoscopic foliation on an equal-area, lower hemisphere stereographic projection (with foliation vertical and stretching lineation horizontal), and contoured using SpheriState 2.2 software.

Quartz *c*-axes from both the Seh-Ghalatoun (Fig. 7A) and the Ghouri outcrops (Fig. 7B) show single girdles. The LPOs from the Ghouri shear zone have maxima concentrated between the *Y*- and *Z*-axes (Fig. 7B). The *c*-axis patterns display both external and internal asymmetries with respect to the foliation (Bahrmann and Platt, 1982; Platt and Behrmann, 1986). According to Law (1990), external fabric asymmetry is defined by the angle of obliquity (ψ) between the central segment of the fabric skeleton and the foliation, whereas the internal asymmetry is defined by the inclination of the central fabric segment to the peripheral segments. The ψ angle of the Seh-Ghalatoun samples is 60°–64°, consistent with a dextral sense of shear.

For two samples the *c*-axis maximum is close to *Y* whereas for two others it is between *Y* and *Z* (Fig. 7A). *Y* maxima such as found in the Ghouri shear zone indicate that prism ⟨a⟩ was the dominant

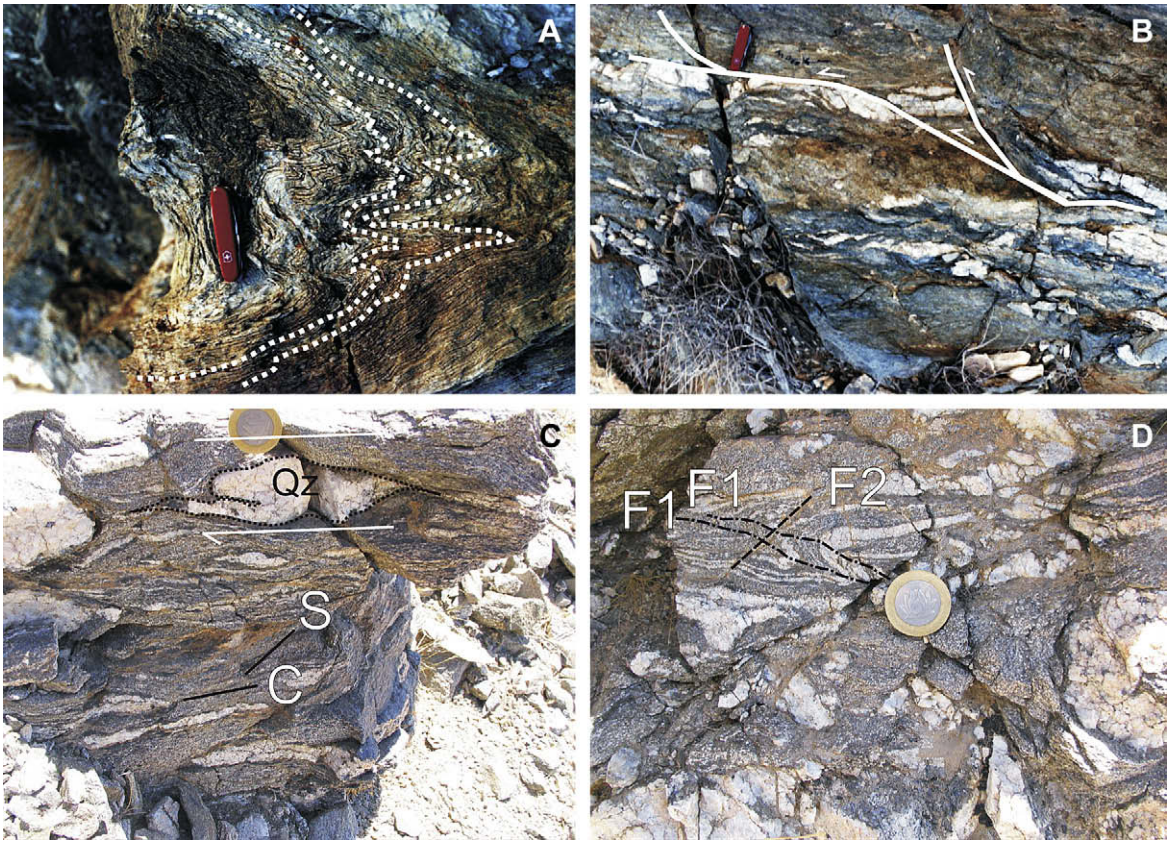

Fig. 5. (A) Seh-Ghalatoun fold profile showing asymmetrical crenulation cleavage of the muscovite schist. (B) Eastern Ghouri quartzite mylonite shear-band boudins showing a long curved lenticular shape and large relative displacement. (C) Seh-Ghalatoun high-grade gneiss showing quartzite with S/C shear bands which display a dextral sense of shear. (D) Asymmetric recumbent type 2 interference folds with wavy outcrop pattern.

slip system (e. g. Wilson, 1975; Bouchez, 1977; Lister and Dornsiepen, 1982), typical for deformation of quartz at moderately high temperature (Schmid and Casey, 1986), e.g. amphibolite facies conditions (Bouchez and Pecher, 1981; Lister and Dornsiepen, 1982; Mainprice et al., 1986; Wenk, 1994).

8. Deformation temperatures

During plastic deformation and dynamic recrystallization, the opening angle of the *c*-axis girdle increases with increasing temperature and/or water content, and decreasing strain rate (Tullis et al., 1973; Lister and Hobbs, 1980; Lister and Dornsiepen, 1982). In the case of plane strain deformation, this opening angle is defined as the angle between two *c*-axis girdles measured in the plane perpendicular to foliation and parallel to lineation (Law et al., 2004). Kruhl (1998) developed a graph of opening angle versus estimated temperature of deformation for a range of greenschist- to granulite-facies environments and demonstrated that at natural strain rates there is an approximately linear increase in opening angle with temperature between 300° and 650 °C (Fig. 8). Kruhl (1998) estimated that for natural deformation, this opening angle "geothermometer" indicates the deformation temperature with an uncertainty of ±50 °C. The underlying assumption in using this geothermometer is that the degree of uncertainty spans the range of strain rates and amounts of hydrolytic weakening likely to be encountered in natural deformation (Law et al., 2004).

Using this geothermometer, the girdle opening angles within the Seh-Ghalatoun high-grade gneisses indicate a mean deformation temperature of 512° ± 50 °C, whereas the girdle opening angles for the Ghouri quartzite mylonite indicate a mean deformation temperature of 485° ± 30 °C. These results indicate that the Ghouri quartzite mylonites were deformed at epidote-amphibolite facies conditions whereas the Seh-Ghalatoun gneisses were deformed at amphibolite facies conditions. Based on a pressure–temperature diagram showing the major metamorphic facies and the geothermal gradient(Turner, 1968), deformation occurred at a depth of about 23–25 km on top of the subducting oceanic crust.

9. Kinematic vorticity number in a microscopic and mesoscopic-scale

The kinematic vorticity number (W_k) is important to measure for quantifying components of pure shear and simple shear in high-strain zones (Means et al., 1980). It is defined (for $0 < W_k < 1$) as a non-linear ratio of pure shear ($W_k = 0$) to simple shear ($W_k = 1$), assuming steady-state deformation (Means, 1994). Several methods have been established to quantify shear-induced vorticity in naturally deformed rocks, including the geometry of LPO patterns of quartz *c*-axes, rotation of porphyroclasts, oblique foliations and the orientation of finite strain with respect to shear zone boundaries (Law et al., 1984; Platt and Behrmann, 1986; Passchier, 1987; Passchier and Urai, 1988; Wallis, 1992; Simpson and De Paor, 1993; Tikoff and Fossen, 1995; Jessup et al., 2007). We have used these in the upper sedimentary mélange and lower metamorphic mélange rocks.

9.1. Method I: strain-ratio/quartz c-axis

Under progressive simple, pure and general shear the central segment of quartz *c*-axis fabrics and active slip system develops

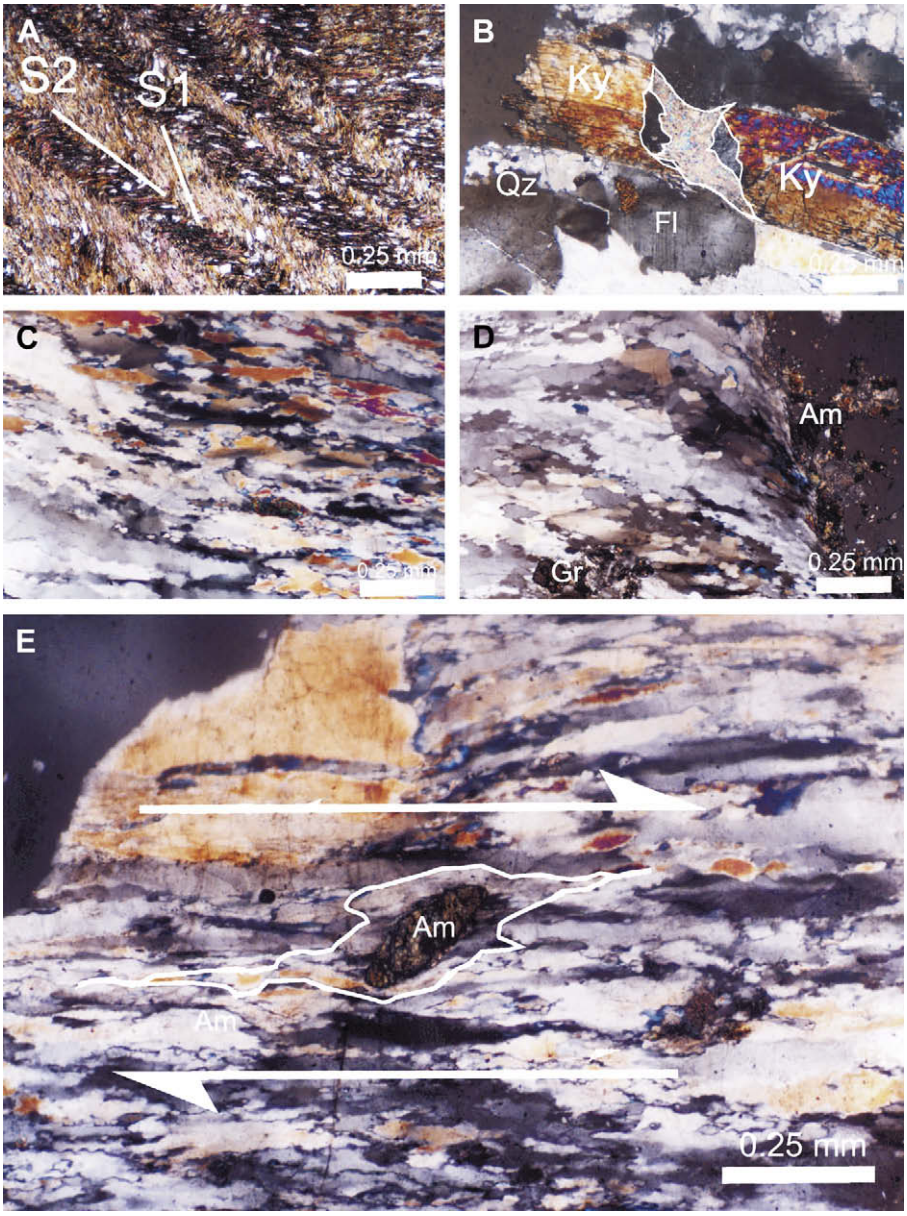

Fig. 6. Optical photomicrographs of the Seh-Ghalatoun muscovite schist, kyanite schist and quartzite mylonite. (A) Muscovite schist showing the S_1 foliation developed during the first phase of the deformation (D_1). This foliation was overprinted by an asymmetric crenulation cleavage (S_2), formed during the second phase of deformation (D_2). (B) Kyanite micro-domino boudins in the kyanite schist (composed of kyanite, feldspar and quartz). Secondary fine-grained muscovite fills the neck of the boudins. (C) Quartzite mylonite showing quartz ribbons formed by flattening of originally equidimensional grains. (D) Curved quartz ribbons and recrystallized quartz grains with an isolated amphibole porphyroclast. (E) Rotated mantled amphibole porphyroclast within quartz ribbons showing δ-type porphyroclast with a dextral sense of shear. The tails of the mantled porphyroclast are composed of strongly elongated quartz grains.

nearly orthogonal to the flow/shear plane (Platt and Behrmann, 1986; Vissers, 1989; Wallis, 1995). This assumption is strongly supported by both experimental (e.g. Bouchez and Duval, 1982; Herwegh et al., 1997) and numerical simulation data (Lister and Hobbs, 1980), as well as observations from naturally deformed rocks (e. g. Law, 1990; Sullivan and Law, 2007). Therefore, the angle β between the perpendicular to the central girdle of quartz *c*-axis fabric and the main foliation is equal to the angle between the flow plane and flattening plane of finite strain (R_{XZ}). Heilbronner and Tullis (2006) have documented a progressive from *Z*-axis maxima to *Y*-axis maxima with increasing strain-induced grain boundary migration recrystallization. This transition occurs because grains oriented preferentially consume other grains during grain boundary migration recrystallization (Hirth and Tullis, 1992). Therefore, it is assumed that there is no dynamic recrystallization, which continuously re-set the LPO. The angle β is a function of R_{XZ} (strain ratio of rotating porphyroclasts; Wallis, 1992) and W_k, as expressed by:

$$W_k = \sin\left\{\tan^{-1}\left[\frac{\sin(2\beta)}{[(R_{XZ}+1)/(R_{XZ}-1)]-\cos(2\beta)}\right]\right\} \times \frac{(R_{XZ}+1)}{(R_{XZ}-1)}$$

This method was applied to seven of the quartz ribbon-bearing mylonites (up to 95% quartz, samples cut perpendicular to foliation and parallel to lineation). The samples have mantled porphyroclasts of amphiboles. These measurements yield an estimated mean kinematic vorticity in the Seh-Ghalatoun outcrop of $W_m = 0.79 \pm 0.011$.

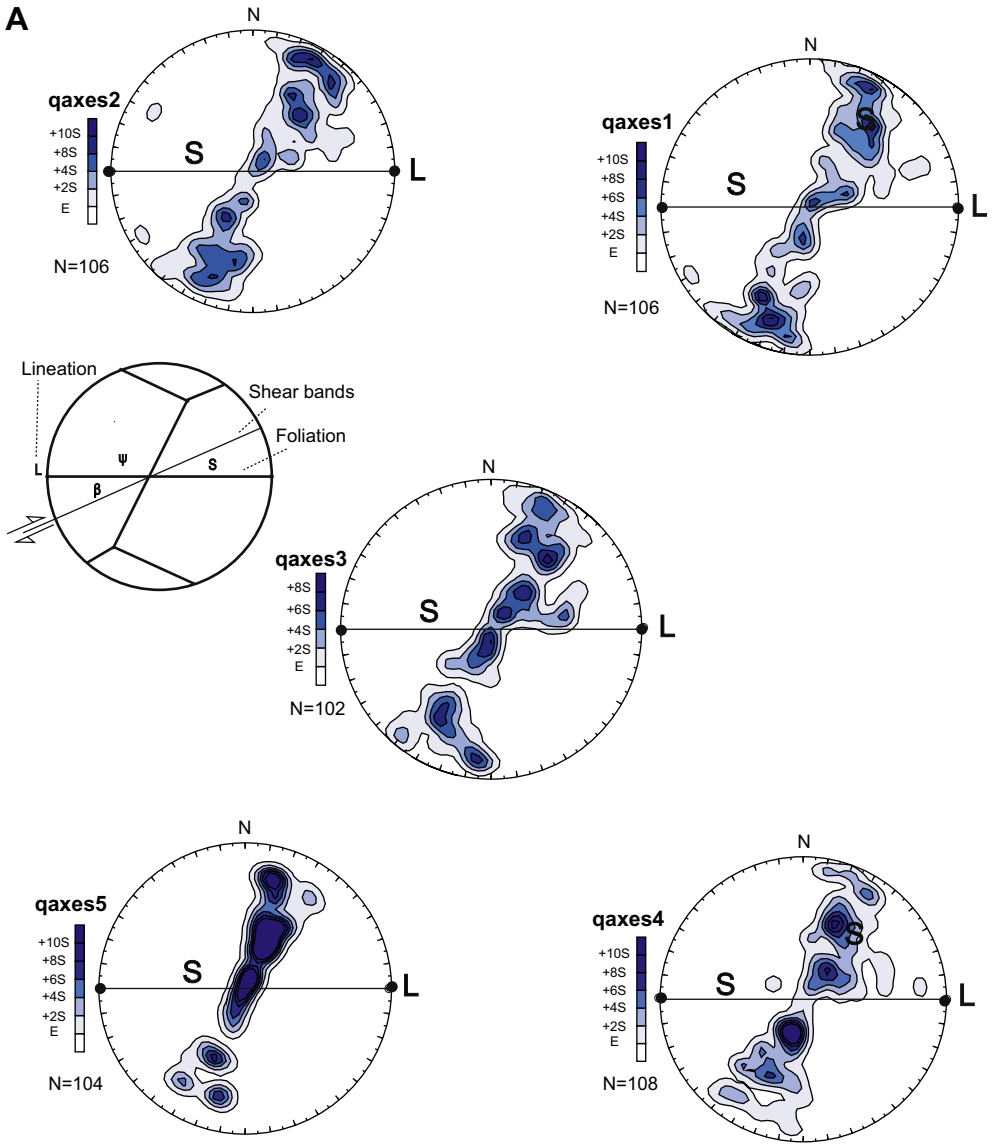

Fig. 7. (A) and (B) Contoured LPO patterns of quartz *c*-axes from the Seh-Ghalatoun gneiss and quartzite mylonite from the northeastern part of the Ghouri shear zone. All projections are equal-area, lower hemisphere. (A) The LPO patterns of the Seh-Ghalatoun rocks show well-developed type-I cross-girdles of *c*-axes with both external and internal asymmetries. (B) The LPO patterns from the eastern Ghouri shear zone have maxima between *Y* and *Z*.

9.2. Method II: the porphyroclast hyperbolic distribution

The use of porphyroclasts to estimate the mean kinematic vorticity (W_m) of a flowing matrix is important for quantifying the relative contributions of pure and simple shear. Several models have been established for the rotation of elliptical objects in a fluid, demonstrating that during simple shear (mean kinematic vorticity number, $W_m = 1$) rigid objects will rotate with increasing contributions of pure shear ($0 < W_m < 1$). Thus porphyroclasts will rotate with a simple-shear component forward or backward until they reach a stable orientation that is unique to R_f (aspect ratio) and W_m (Jessup et al., 2007; Ghosh and Ramberg, 1976).

Simpson and De Paor (1993, 1997) proposed the porphyroclast hyperbolic distribution method for estimating the kinematic vorticity number. The method is based on the premise that the orientation of the long axes of backward rotated mesoscopic porphyroclasts within the acute angle field between the flow eigenvectors delineates the orientation of the unstable eigenvector. The stable eigenvector is assumed to be normal to the foliation (Simpson and De Paor, 1997). The angle between the long axis of the mesoscopic porphyroclasts of the type-I sedimentary mélange and quartzo-feldspathic gneiss was measured relative to the shear zone boundary or foliation. Axial ratios (R_f) of the porphyroclasts were also measured. Both the angle and axial ratio were plotted on a hyperbolic stereonet (Simpson and De Paor, 1993). The hyperbola represent the acute angle between two eigenvectors, such that cosine of this angle (v) yields the mean kinematic vorticity number (Bobyarchick, 1986) $W_m = \cos(v)$.

41 samples of mesoscopic porphyroclasts of the type-I upper sedimentary mélange (Fig. 9A) along the Zagros thrust system and 51 samples of quartzo-feldspathic porphyroclasts from the Seh-Ghalatoun (Fig. 9B) were analyzed by the modified porphyroclasts hyperbolic distribution method. The samples from the type-I sedimentary mélange and those from the quartzo-feldspathic porphyroclasts yield in the lineation-parallel section (*XZ*-plane) $W_m = 0.766$ and $W_m = 0.866$, respectively, indicating general shear.

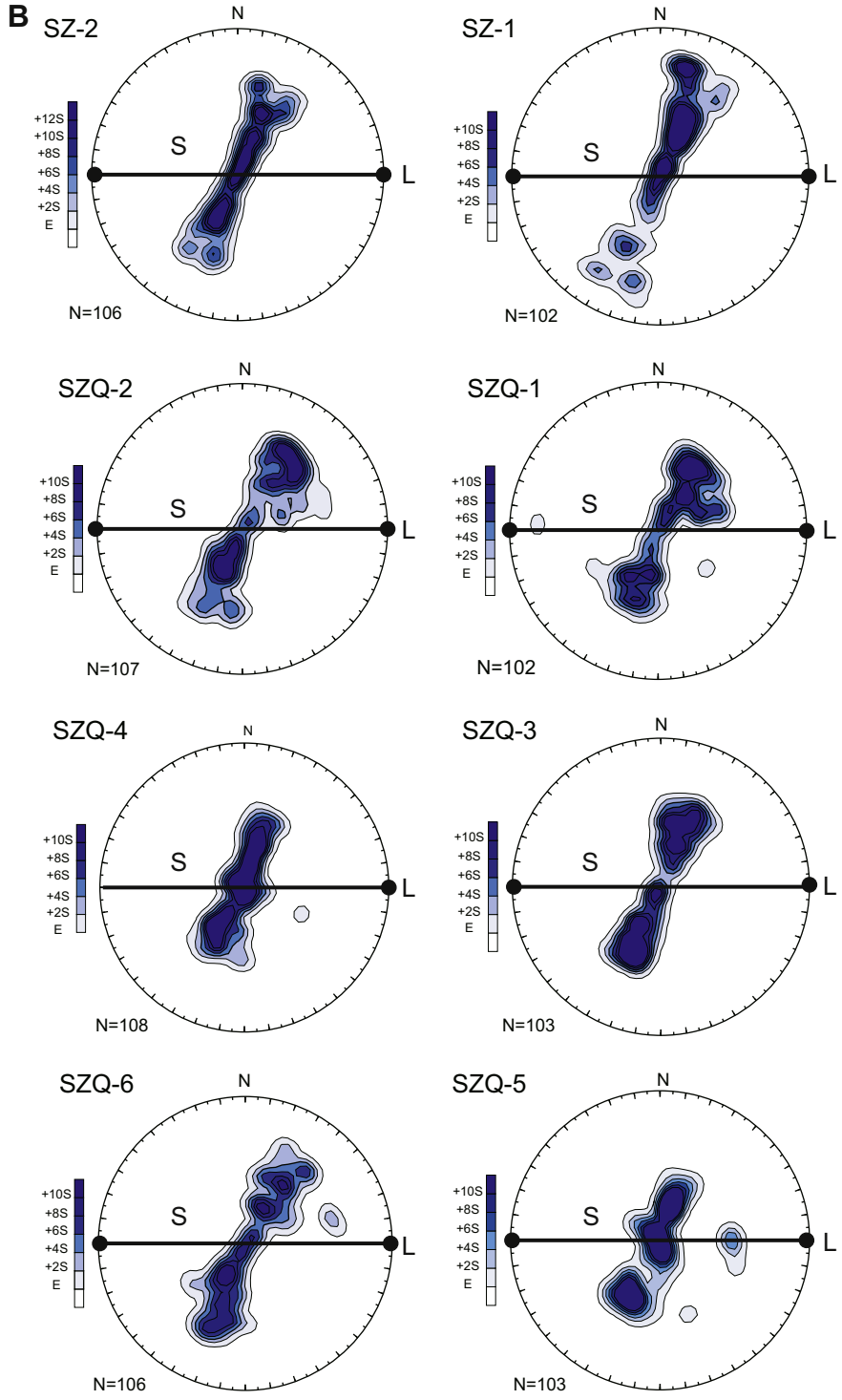

Fig. 7. (*continued*).

9.3. Method III: the rigid grain net (RGN)

Analytical techniques of Passchier (1987), Simpson and De Paor (1993, 1997) and Wallis (1995) use rigid porphyroclasts to estimate W in high-strain zones, all of which rely on the same fundamental relationships between W_m (mean kinematic vorticity number) and B^* (shape factor), through the following equation:

$$B^* = \left(\mathrm{Mx}^2 - \mathrm{Mn}^2\right) \Big/ \left(\mathrm{Mx}^2 + \mathrm{Mn}^2\right)$$

where Mn, short axis of clast; Mx, long axis of clast, and theta = angle of porphyroclasts long axis with respect to the macroscopic foliation (θ). This relation defines a critical threshold (Rc) below which porphyroclasts continually rotate, and above which they

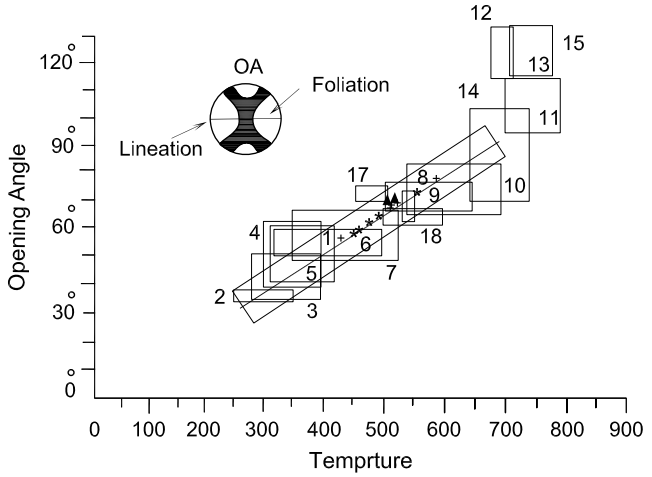

Fig. 8. Diagram showing effect of temperature of deformation on the opening angle of small circle patterns of quartz *c*-axes. The estimated temperatures of deformation for eighteen naturally deformed rocks at different metamorphic grade are shown as Kruhl (1998); indicate data from Law et al. (1992), Nyman et al. (1995) and Okudaira et al. (1995), respectively. The best fit straight-line relationship between opening angle and temperature is indicated for localities with deformation temperature <650 °C; oblique rectangle indicates confidence limit of ±50° (Law et al., 2004).

record a stable-sink orientation (Ghosh and Ramberg, 1976; Jessup et al., 2007). To explore this relationship, Jessup et al. (2007) proposed the Rigid Grain Net (RGN) program as an alternative graphical method for estimating W_m. The RGN contains semi-hyperbolas that are the mathematical equivalents to the hyperbolic net used for the porphyroclast hyperbolic distribution method. The RGN plot of the type-I sedimentary mélange (Fig. 9C) and quartzo-feldspathic porphyroclasts (Fig. 9D) yields $W_m = 0.88$ and $W_m = 0.89$, respectively.

Comparison of methods I, II and III indicate that the RGN method gives higher estimated mean W_m values, especially for the Seh-Ghalatoun outcrop. These differences may reflect uncertainties in the analyses, or perhaps the W_k values may record different parts of the deformation history in different outcrops, or different rates of rigid block rotation. In natural systems, the vorticity of flow may vary with both position and time (Fossen and Tikoff, 1998; Jiang, 1998). W_k may change during progressive deformation, and therefore most methods determine a mean value over time, termed W_m (Passchier and Trouw, 2005). The estimated mean $W_k = W_m$ of the all methods is 0.84 ± 0.05.

10. $^{40}Ar/^{39}Ar$ step-heating analytical technique

$^{40}Ar/^{39}Ar$ analyses of oriented biotite samples (KS11-S1, KS5-S7 and KS8-S8), a muscovite sample (KS5-S7) and amphibole samples (KS2-AM10 and KS4-AM12) from the Seh-Ghalatoun biotite gneiss and amphibolite outcrops were undertaken at Queen's University, Canada, following standard methods (e.g. McDougall and Harrison, 1988). The mineral separates were obtained by crushing hand-sized samples, sieving and passing 700 μm and 2 mm fractions through heavy liquids. The mineral concentrates were further purified (to >99%) by ultrasonic washing in water and hand-picking. Samples were irradiated in the nuclear reactor at McMaster

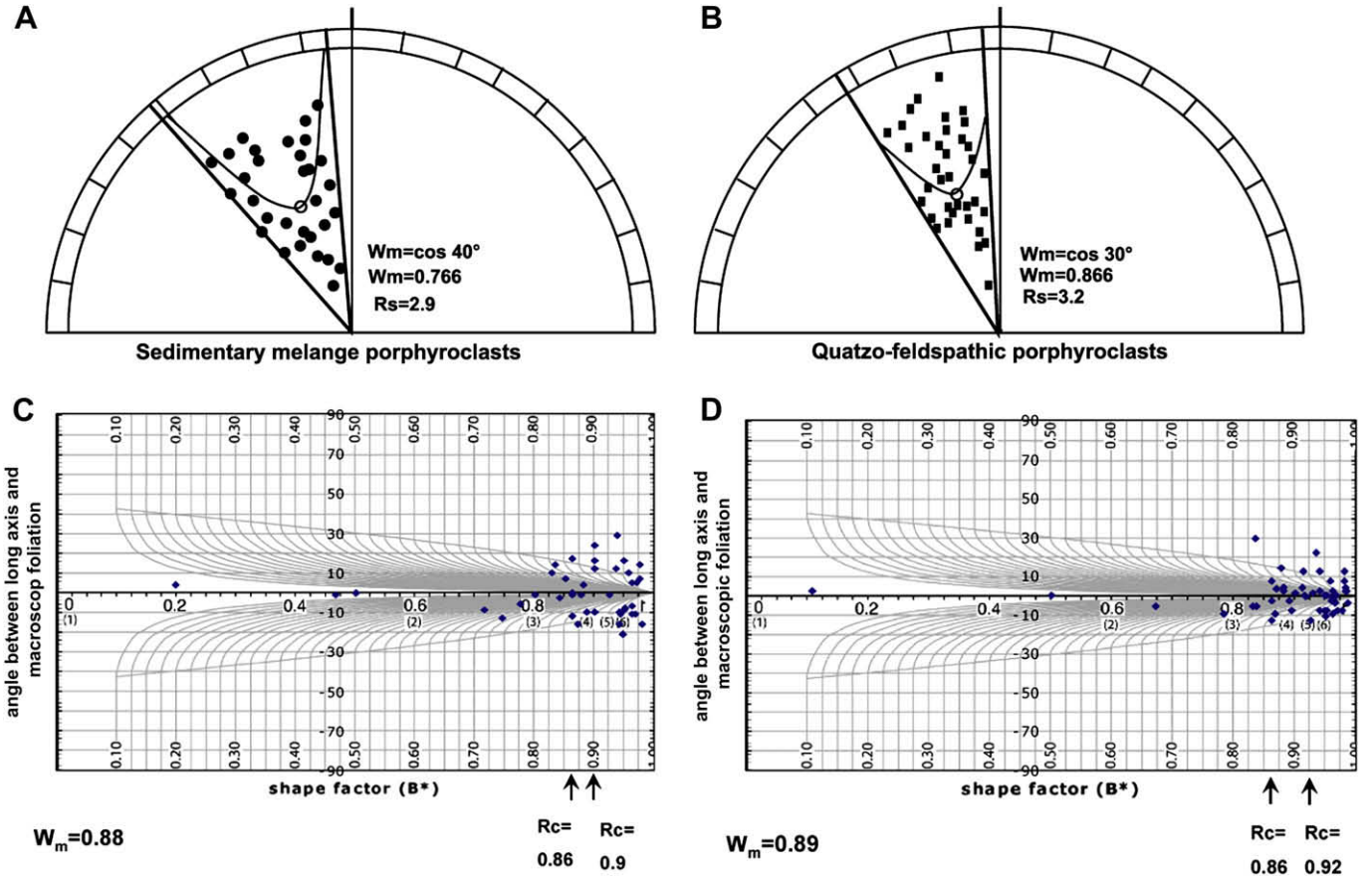

Fig. 9. (A and B) Plots of kinematic vorticity data of the porphyroclasts from the upper sedimentary mélange and Seh-Ghalatoun metamorphic mélange on a half of the hyperbolic net. Stable eigenvectors are shown as lines. (C and D) Plots of kinematic vorticity data of the porphyroclasts of the upper sedimentary mélange and Seh-Ghalatoun metamorphic mélange on the Rigid Grain Net (RGN) using semi-hyperbolas.

University in Hamilton (Canada), in position 5C for 10 h to transform a portion of K to ^{39}Ar through the interaction of fast neutrons.

Samples were heated with an argon-ion laser. Laser step heating was done with a defocused beam by changing the output of the laser from 0.75 W to 7 W. Total fusion was done in the last step by changing the focusing lens of the 7.0 W laser beam. Gas was expanded into a stainless steel clean-up line purified with two 101/s SAES gathers. Argon was analyzed isotopically using a 216 MAP mass spectrometer. Data were corrected for machine background determined by measuring system blanks, and mass discrimination by analyzing atmospheric argon.

10.1. $^{40}Ar/^{39}Ar$ biotite and muscovite results

Interpreting ^{40}Ar/^{39}Ar dates from deformed and metamorphosed terranes is difficult. Among samples from the same terrane, variations in thermal history, deformation history, lithology, and exposure to excess argon may account for variations in ^{40}Ar/^{39}Ar dates (Markley et al., 2002).

^{40}Ar/^{39}Ar step-heating experiments of single 2 mm biotite grain of the biotite gneiss (Ks11-S1) yielded an age spectrum in which all 8 steps (99.8% of total ^{39}Ar released) define a plateau with weighted mean age of 119.95 ± 0.88 Ma. Grouping the medium-grained biotite from the biotite gneiss (KS5-S7) yielded a plateau including 9 steps (71.4% of the total ^{39}Ar released) that gives a weighted mean age of 112.58 ± 0.66 Ma (Fig. 10A). Medium-grained muscovite from muscovite and biotite schist sample KS8-S8 yielded a flat age spectrum including 7 of 9 steps (74.8% of total ^{39}Ar released) with a well-defined plateau yielding a weighted mean age of 83.09 ± 0.38 Ma.

Two biotite spectra exhibit characteristics common to many biotite ^{40}Ar/^{39}Ar step-heating spectra worldwide. The relationship between the ^{40}Ar/^{39}Ar date and grain size may constrain interpretations of the dates (Turner, 1968; Lovera et al., 1989).

(1) Variations in thermal history, deformation history, lithology (Markley et al., 2002).
(2) Incorporation of excess argon through intragrain diffusion (Harrison and McDougall, 1981; Pickles et al., 1997) or trapped within fluid inclusions and/or mineral phases (Kelley, 2002), or coexisting biotite populations (York and Lopez Martinez, 1986).
(3) Recoil-induced $^{39}Ar_k$ redistribution and differential release from interlayered chlorite (Lo and Onstott, 1989) and/or other fine-grained minerals (Dong et al., 1997) during step-heating, and deformation-induced dislocations or sub-grain networks that alter argon diffusivity, retentivity and/or susceptibility to dehydroxylation reactions (Kramar et al., 2001; Foster and Lister, 2004).

10.2. $^{40}Ar/^{39}Ar$ amphibole results

Two groups of coarse-grained amphiboles from the Seh-Ghalatoun amphibolite samples (KS2-AM10 and KS4-AM12) measured using the step-heating method give plateau ages of 89.09 ± 1.34 Ma and 90.18 ± 0.88 Ma (all errors $\pm 1\sigma$). The combination of 14 steps of the sample isochron ages (62.8% of the total ^{39}Ar released) gives a weighted mean age of 91.23 ± 0.89 Ma (Fig. 10B).

Two coarse-grained amphiboles with a mean age of 91.23 ± 0.89 Ma display fairly similar age spectra. These small variations in age could be due to: (1) very minor, optically undetectable mineralogical contaminants in amphibole concentrates; (2) petrographically unresolvable exsolution or compositional zonation within constituent amphibole grains, (3) minor chlorite replacement of hornblende, and/or (4) intracrystalline inclusions (Wilson et al., 2000).

Previous K–Ar age spectra obtained from biotite and hornblende of the biotite schist and garnet amphibolite in this area yielded $\sim 87 \pm 7$ Ma and 96 ± 1.3 Ma (Haynes and Reynolds, 1980). Lanphere and Pamic (1983) also measured ^{40}Ar/^{39}Ar amphibole from the diabase, and obtained ages of 85.9 ± 3.8 Ma and 83.6 ± 8.4 Ma. The weighted mean age of hornblende from five hornblende samples from the Neyriz ophiolite is 87.5 ± 7.2 Ma (Lanphere and Pamic, 1983).

11. Discussion

11.1. Characteristics of the Zagros accretionary prism

The fabrics of the Hassan Abad upper sedimentary mélange and Seh-Ghalatoun lower metamorphic mélange along the Neyriz ophiolite show characteristics of a classical accretionary prism, including type-I mélange with S-, C-, and Ć-type shear-band cleavages; type-II mélange with stretching lineations defined by ribbons, stripes, rods or flattened lenses of greywacke or limestone; and type-III mélange with rectangular, fish-head, or barrel-shaped boudins set in a shale or mudstone matrix. The type-II and type-III mélanges were formed by sub-horizontal layer–parallel extension, which has been explained by two models: (1) gravity-driven slumping or sliding of surfacial slope sediments covering the prism (e.g. Cowan, 1985), or (2) layer-parallel shear during vertical loading of sediments in and below the decollement (Fisher and Byrne, 1987; Brown and Behrmann, 1990; Kusky and Bradley, 1999). A number of studies have shown that components of horizontal stretching are associated with lateral extrusion of the deformation zone (Harland, 1971; Jones et al., 1997). Shear zones accommodating the lateral escape of large lithospheric fragments may undergo a component of lateral extrusion (Teyssier and Tikoff, 1999). Significant components of simple shear relative to pure shear may be involved in the inclined lateral exhumation of high-grade metamorphic rocks. Passchier (1998) proposed "non-simple-shear zones" or "general shearing" (Simpson and De Paor, 1993) or transpression (Sanderson and Marchini, 1984) for fabrics resulting from simultaneous simple and pure shear. Modeling of finite strain accumulation shows that combinations of simple and pure shear are associated with strike slip and oblique convergent systems (Tikoff and Teyssier, 1994). Exhumation of high-grade metamorphic rocks (such as eclogite, blueschist, garnet amphibolite and kyanite schist) produced the wedge-shaped Sanandaj-Sirjan HP–LT metamorphic belt (Sarkarinejad, 2007). Simultaneous strike slip and dip slip may occur especially in orogenic belts which have wedge-shaped geometries and non-planar zone boundaries (Jones et al., 2004).

11.2. Inclined lateral flow and stretching lineation

The presence in the lower metamorphic mélange unit of amphibolite and garnet amphibolite, which contain boudins of eclogite and slices of blueschist, provides kinematic indicators suggesting simultaneous strike slip and dip slip and shear zones which allow inclined lateral exhumation of high-pressure rocks to the top of the subduction zone. In the amphibolites, the dominant sub-horizontal mineral stretching lineation L_1 (25°, N 3° W) and the moderate foliation (N 54° W, 58° NE) confirm the inclined lateral exhumation of the high-pressure metamorphic rocks.

11.3. Rotation of blocks within the prism

The estimated mean kinematic vorticity number (W_k) based on several indicators is 0.84. According to Fossen and Tikoff (1993),

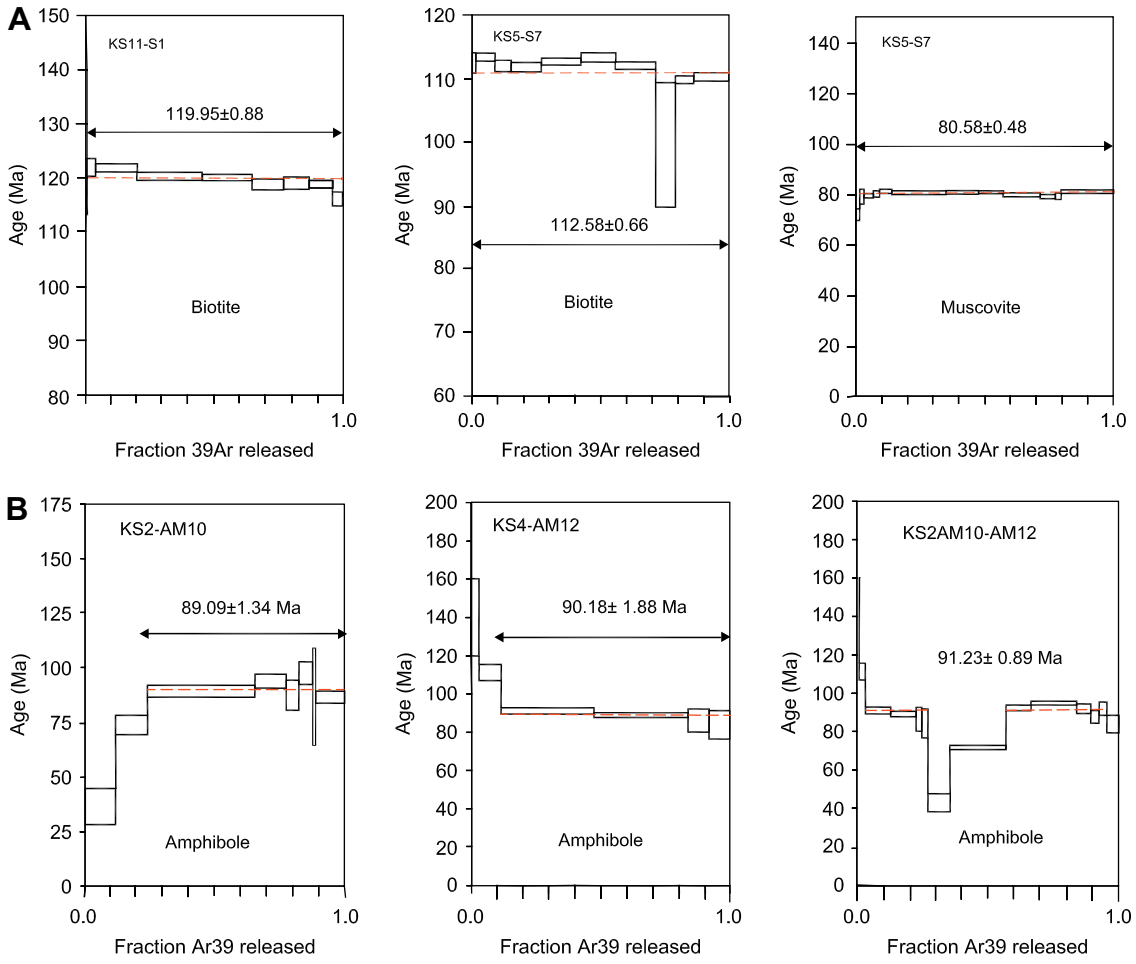

Fig. 10. Laser step-heating $^{40}Ar/^{39}Ar$ spectrum for coarse single grained biotite (KS11-S1), medium-grained biotite and muscovite samples (KS5-S7) of the Seh-Ghalatoun biotite gneiss. (B) Laser step-heating spectrum for amphibole (KS2-AM10 and KS4-AM12) and combination of KS2-AM10 and KS4-AM12 isochron ages of 14 steps.

there is a relationship between W_k and the angle θ between the maximum horizontal axis of the instantaneous strain ellipsoid (s_1) and the deformation zone boundaries. Using W_k values, the estimated θ angle for the Zagros accretionary prism is 37°, characteristic of wrench-dominated transpression. Wrench-dominated transpression is indicated when $1 > W_k > 0.81$ and $35° < \theta < 45°$ (Fossen and Tikoff, 1993). In such cases s_1 and s_3 (maximum and minimum axes of the instantaneous strain ellipsoid) lie in a horizontal plane, and strike slip and thrust faults both continue to be active during deformation and accommodate transcurrent and contractional components of deformation (Tikoff and Teyssier, 1994). Applying the relationship between θ and α, the estimated value for α in the Zagros accretionary prism based on the kinematic vorticity number is 18.5°. This is the mean angle of plate convergence in the tectonic wedge, and varies from 23° in the upper tectonic sedimentary mélange unit to 11° in the lower high-pressure metamorphic mélange unit. Possible reasons for different kinematic vorticity numbers and variations of the α angle include different rates of rotation and clockwise and counterclockwise rotations of rigid blocks on top of the NE-dipping Neo-Tethyan subducting plate.

The block rotations in the upper sedimentary mélange unit are clockwise. However the quartz *c*-axis patterns and meso-scale sheared or rotated boudins indicate counterclockwise rotation.

The opening angle of quartz *c*-axis fabrics has been used to determine the active slip system and indirectly the temperature of deformation, with an estimated accuracy of ±50 °C (Kruhl, 1998; Law et al., 2004). The inferred deformation temperature varies from 485° ± 30 °C to 512° ± 50 °C. The upper part of the wedge has a lower temperature of deformation (geothermal gradient, strain rate) and the ductile lower crust and mantle at depth have a higher temperature.

11.4. Simple-shear and pure-shear components of deformation

The estimated mean kinematic vorticity number determined by different methods yields W_m values of 0.84 ± 0.05. In natural systems, the vorticity of flow may vary with both position and time (Fossen and Tikoff, 1998; Jiang, 1998). In such cases of non-steady-state deformation, flow is more appropriately characterized by the mean kinematic vorticity number W_m, in which the vorticity of flow is integrated over space and time (Passchier, 1988). W_k (instantaneous deformation) is equal to W_m (finite deformation) for steady-state deformation (Law et al., 2004). The mean estimated finite deformation (W_m) value indicates 39.5% pure shear and 60.5% simple shear (Fig. 11; corresponding to $W_k = W_m = 0.84$).

11.5. $^{40}Ar/^{39}Ar$ interpretation

$^{40}Ar/^{39}Ar$ step-heating measurements on the biotite and muscovite from the biotite gneiss of the Seh-Ghalatoun lower metamorphic mélange are consistent with the overprinting relationship determined from field observations. The first generation of foliation (S_1) has a NW–SE orientation with a moderate NE dip.

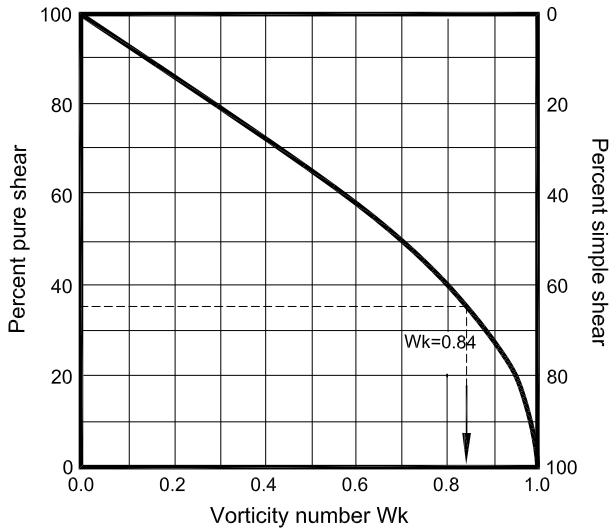

Fig. 11. Diagram showing the non-linear relationship between kinematic vorticity numbers of pure and simple shear for instantaneous 2D flow. W_k is defined as a non-linear ratio of the pure-shear ($W_k = 0$) and simple-shear ($W_k = 1$) components of deformation, assuming a steady-state deformation (Means, 1994).

The first generation of biotite yields plateau ages of 119.95 ± 0.88 Ma and 112.58 ± 0.66 Ma. These late Aptian ages are related to early thrusting and formation of high-pressure metamorphic rocks at the peak of metamorphism prior to formation of the Neyriz ophiolite. The ages we determined are consistent with other age-constraint data from the Oman ophiolite. The Neyriz and Oman ophiolites were originally parts of the Neo-Tethyan oceanic lithosphere and were separated during the late Cretaceous by collision of the Iranian microcontinent with the Afro-Arabian continent (Sarkarinejad, 2005). $^{40}Ar/^{39}Ar$ apparent ages of the exhumation-related fabrics of glaucophone-bearing eclogites of the Oman continental margin as distinct metamorphic/cooling intervals of 140–135, 120–98 and 92–80 Ma (Gray et al., 2004a) and 110 ± 9 and 109 ± 13 Ma ages interpreted the timing of prograde, peak of high-pressure metamorphism in the rocks that are structurally beneath the Samail ophiolite (Gray et al., 2004b).

$^{40}Ar/^{39}Ar$ incremental-heating of amphibole from the Seh-Ghalatoun amphibolite gives isochron ages of 89.09 ± 1.34 Ma and 90.18 ± 1.88 Ma or a weighted mean age of 91.23 ± 0.89 Ma. This Turonian–Cenomanian age indicates subduction and obduction of the Neyriz ophiolite and later lateral extrusion and exhumation of the high-pressure metamorphic rocks such as eclogite and blueschist along the Zagros accretionary prism. Reconstruction of ophiolite emplacements in Turkey and Oman along the Alpine–Himalayan orogenic belt confirms synchronous ophiolite emplacement. $^{40}Ar/^{39}Ar$ step-heating measurements on amphibole from the Mersin ophiolite (southern Turkey) give a weighted mean age of 92.6 ± 0.2 (Parlak and Delaloye, 1999). Other $^{40}Ar/^{39}Ar$ hornblende ages indicate that amphibolite facies deformation and metamorphism of the sole thrust were completed by 93.7 ± 0.8 Ma (Hacker, 1994).

12. Summary and conclusions

(1) The presence of an upper sedimentary mélange and a lower metamorphic mélange, exposing HP–LT metamorphic rocks along the Neyriz ophiolite, provides evidence of an ancient accretionary prism. Type-I mélange displays S-, C- and C′-type shear-band cleavages; type-II mélange contains a stretching lineation defined by ribbons, stripes or rods or flattened lenses of greywacke or limestone; type-III mélange includes rectangular, fish-head or barrel-shaped boudins set in a matrix of shale or mudstone. The lower metamorphic mélange displays eye- and sigmoidal-shaped and winged σ-type and δ-type porphyroclasts, indicating non-planar rotation during transpression.

(2) The dominant HP–LT metamorphic rocks such as amphibolite and garnet amphibolite, which contain continuous to discontinuous rotated shear-band boudins of eclogite and slices of blueschist in the lower metamorphic mélange unit, provide kinematic indicators suggesting simultaneous strike slip and dip slip, and shear zones allowing inclined lateral exhumation of the high-pressure rocks of oceanic and continental crustal origin to the top of the subduction zone along the marginal boundaries of the inclined transpression zone.

(3) The estimated mean kinematic vorticity number (W_m) based on quartz *c*-axis patterns and rotating porphyroclasts in a flowing matrix is 0.84. There is a relationship between W_k and the angle θ between the maximum horizontal axis of the instantaneous strain ellipsoid (s_1) and the deformation zone boundary. Using W_k values, the estimated θ angle for the Zagros accretionary prism is 37°, which is characteristic of wrench-dominated transpression.

(4) The mean estimated finite deformation (W_m) value indicates 39.5% pure shear (corresponding to $W_k = W_m = 0.84$) and 60.5% simple shear. Deformation thus involved simultaneous strike slip and dip slip, and exhumation of the HP–LT rocks along an inclined convergent boundary. $^{40}Ar/^{39}Ar$ step heating of amphibole from the amphibolite gives isochoron ages of 89.09 ± 1.34 Ma and 90.18 ± 1.88 Ma, or a weighted mean age of 91.23 ± 0.89 Ma. This Turonian–Cenomanian age indicates convergence of the Afro-Arabian continent with the Iranian microcontinent and closure of the Tethyan Ocean, leading to obduction of the Neyriz ophiolite and later lateral extrusion and exhumation of the high-pressure metamorphic rocks of the Sanandaj-Sirjan HP–LT metamorphic belt parallel with the NW–SE trending Zagros thrust system.

Acknowledgements

The authors wish to thank an anonymous reviewer who critically reviewed the manuscript and made valuable suggestions for its improvement. We are grateful to Professor Jan Tullis for critical reading and contributing valuable suggestions, which greatly improved the presentation. Thanks also to Professor Joao Hippertt for a constructive review and editorial comments. The first author wishes to thank Dr. Doug Archibald, for providing technical advice for $^{40}Ar/^{39}Ar$ geochronology analysis of the biotite gneiss and amphibolite samples, during sabbatical leave at the Queen's University, Canada. Thank to Abdolreza Partabian, Saadieh Keshavarz and Shahram Kargar for their help in the field and laboratory. This research was supported by the Shiraz University Research Council (SURC) grant which is gratefully acknowledged.

References

Alavi, M., 1994. Tectonics of the Zagros orogenic belt of Iran: new data and interpretation. Tectonophysics 229, 211–238.

Bahrmann, J.H., Platt, J.P., 1982. Sense of nappe emplacement from quartz *c*-axis fabrics: an example from the Betic Cordilleras (Spain). Earth and Planetary Science Letters 59, 208–215.

Berberian, M., King, G.C.P., 1981. Towards a paleogeography and tectonic evolution of Iran. Canadian Journal of Earth Sciences 18, 210–265.

Berthe, D., Choukroune, P., Jegouzo, P., 1979a. Orthogneiss, mylonite and non-coaxial deformation of granites, the example of the South Armorican shear zone. Journal of Structural Geology 1, 31–42.

Berthe, D., Choukroune, P., Gapais, D., 1979b. Orientations préférentielles du quartz et orthogneiss progressive en régime cisaillant: l example due cisaillement sud-armorican. Bulltin Minéralogy 102, 265–272.

Bobyarchick, A.R., 1986. The eigenvalues of steady-state flow in Mohr space. Tectonophysics 122, 33–35.
Bouchez, J.L., 1977. Plastic deformation of quartzites at low temperature in an area of natural strain gradient. Tectonophysics 39, 25–50.
Bouchez, J.L., Duval, P., 1982. The fabric of polycrystalline ice deformed in simple shear: experiments in torsion, natural deformation and geometrical interpretation. Texture and Microstructures 5, 171–190.
Bouchez, J.L., Pecher, A., 1981. The Himalayan Main Central Thrust pile and its quartz-rich tectonites in Central Nepal. Tectonophysics 78, 23–50.
Brown, K.M., Behrmann, J.H., 1990. Genesis and evolution of small-scale structures in the toe of the Barbados Ridge accretionary wedge. Proceedings of the Ocean Drilling Program: Scientific Results 110, 229–244.
Chi, W.C., Reed, D.R., Moore, G., Nguyan, T., Liu, C.S., Lundberg, N., 2003. Tectonic wedging along the rear of the offshore Taiwan accretionary prism. Tectonophysics 374, 199–217.
Cowan, D.S., 1985. Structural styles in Mesozoic and Cenozoic mélanges in western Cordillera of North America. Geological Society of America Bulletin 96, 451–462.
Dong, H., Hall, C.M., Halliday, A.N., Peacor, D.R., Merriman, R.J., Roberts, B., 1997. $^{40}Ar/^{39}Ar$ illite dating of Late Caledonian (Acadian) metamorphism and cooling of K-bentonites and slates from the Welsh Basin, UK. Earth and Planetary Science Letters 150, 337–351.
Falcon, N.L., 1974. Southern Iran: Zagros Mountains. In: Spencer, A.M. (Ed.), Mesozoic–Cenozoic Orogenic Belts, Data for Orogenic Studies. Geological Society of London, Special Publication, pp. 199–211.
Fisher, D., Byrne, T., 1987. Structural evolution of underthrusted sediments, Kodiak Island, Alaska. Tectonics 3, 23–29.
Fossen, H., Tikoff, B., 1998. Forward modeling of non-steady-state deformations and the "minimum strain path": reply. Journal of Structural Geology 20, 979–981.
Fossen, H., Tikoff, B., Teyssier, C., 1994. Strain modeling of transpression and transtension deformation. Norsk Geologisk Tidsskrift 74, 134–145.
Fossen, H., Tikoff, B., 1993. The deformation matrix for simultaneous simple shearing, pure shearing and volume change, and its application to transpression–transtension tectonics. Journal of Structural Geology 15, 413–422.
Foster, M.A., Lister, G.S., 2004. The interpretation of $^{40}Ar/^{39}Ar$ apparent age spectra produced by mixing: application of the method of asymptotes and limits. Journal of Structural Geology 26, 287–305.
Gansser, A., 1974. The ophiolitic mélange, a world-wide problem on Tethyan example. Eclogae Geologicae Helvetiae 67, 479–507.
Ghosh, S.K., Ramberg, H., 1976. Reorientation of inclusions by combination of pure shear and simple shear. Tectonophysics 34, 1–70.
Goscombe, B., Passchier, C.W., Hand, M., 2004. Boudinge classification: end-member boudin types and modified boudin structures. Journal of Structural Geology 26, 739–763.
Goscombe, B., Passchier, C.W., 2003. Asymmetrical boudins as shear sense indicators as field assessment from field data. Journal of Structural Geology 25, 575–589.
Gray, D.R., Hand, M., Mawby, J., Armstrong, R.A., McL, J., Gregory, R.T., 2004a. Sm–Nd and zircon U–Pb ages from garnet-bearing eclogites, NE Oman: constraints on high-P metamorphism. Earth and Planetary Science Letters 222, 407–422.
Gray, D.R., McL, J., David, A., Foster, R., Gregory, T., 2004b. Transition from subduction- to exhumation-related fabrics in glaucophane-bearing eclogites, Oman: evidence from relative fabric chronology and $^{40}Ar/^{39}Ar$ ages. Tectonophysics 389, 35–64.
Hacker, B.R., 1994. Rapid emplacement of young oceanic lithosphere: argon geochronology of the Oman ophiolite. Science 265, 1563–1565.
Harland, W., 1971. Tectonic transpression in Caledonian Spitzbergen. Geological Magazine 108, 27–42.
Harrison, T.M., McDougall, I., 1981. Excess ^{40}Ar in metamorphic rocks from Broken Hill, New South Wales: implications for $^{40}Ar/^{39}Ar$ age spectra and thermal history of the region. Earth and Planetary Science Letters 55, 123–149.
Haynes, S.J., Reynolds, P.H., 1980. Early development of Tethys and Jurassic ophiolite displacement. Nature 283, 561–563.
Haynes, S.J., McQuillan, H., 1974. Evolution of the Zagros Suture zone, southern Iran. Geological Society of America Bulletin 85, 739–744.
Heilbronner, R., Tullis, J., 2006. Evolution of *c*-axis pole figures and grain size during dynamic recrystallization; results from experimentally sheared quartzite. Journal of Geophysical Research 111, B102202. doi:10.1029/2005JB004194.
Herwegh, M., Handy, M.R., Heilbronner, R., 1997. Temperature- and strain rate-dependent microfabric evolution in monomineralic mylonite: evidence from in-situ deformation of norcamphor. Tectonophysics 280, 83–106.
Hirth, G., Tullis, J., 1992. Dislocation creep regimes in quartz aggregates. Journal of Structural Geology 14, 145–159.
Jackson, J.A., Mckenzie, D.P., 1984. Active tectonics of the Alpine–Himalayan Belt between western Turkey and Pakistan. Geophysical Journal Review of Royal Astronomical Society 77, 185–246.
Jessup, M.J., Law, R.D., Frassi, C., 2007. The rigid grain net (RGN): an alternative method for estimating mean kinematic vorticity number (W_m). Journal of Structural Geology 29, 411–421.
Jiang, D., 1998. Forward modeling of non-steady-state deformations and the "minimum strain path". Discussion. Journal of Structural Geology 20, 975–977.
Jones, R.R., Holdsworth, R.E., Clegg, P., McCaffrey, K., Tavarnell, E., 2004. Inclined transpression. Journal of Structural Geology 26, 1531–1548.
Jones, R.R., Holdsworth, R.E., 1998. Oblique simple shear in transpression zones. In: Holdsworth, R.E., Strachan, R.A., Dewey, J.F. (Eds.), Continental Transpressional and Transtensional Tectonics. Special Publication of the Geological Society, London, vol. 135, pp. 35–40.
Jones, R.R., Holdsworth, R.E., Baily, W., 1997. Lateral extrusion in transpression zones: the importance of boundary conditions. Journal of Structural Geology 19, 1201–1217.
Jones, R.R., Tanner, P.W.G., 1995. Strain partitioning in transpression zones. Journal of Structural Geology 17, 793–802.
Kelley, S., 2002. Excess argon in K–Ar and Ar–Ar geochronology. Chemical Geology 188, 1–22.
Kramar, N., Cosca, M., Hunziker, J.C., 2001. $^{40}Ar_*$ distributions in naturally deformed muscovite: in situ UV-laser ablation evidence for microstructurally intragrain diffusion. Earth and Planetary Science Letters 192, 377–388.
Kruhl, J.H., 1998. Prism- and basal-plane parallel subgrain boundaries in quartz: a microstructural and geotheromobarometer. Journal of Metamorphic Geology 14, 581–589.
Kusky, T.M., Bradley, D.C., 1999. Kinematic analysis of mélange fabrics: examples and applications from the McHugh complex, Kenai Peninsula, Alaska. Journal of Structural Geology 21, 1773–1796.
Lanphere, M.A., Pamic, J., 1983. $^{40}Ar/^{39}Ar$ ages and tectonic setting of ophiolite from the Neyriz area, southwest Zagros range, Iran. Tectonophysics 96, 245–256.
Law, R.D., 1990. Crystallographic fabrics: a selective review of their applications to research in structural geology. In: Knipe, R.J., Rutter, E.H. (Eds.), Deformation Mechanisms, Rheology and Tectonics. Geological Society Special Publication, vol. 54, pp. 335–352.
Law, R.D., Searle, M.P., Simpson, R.L.O., 2004. Strain, deformation temperatures and vorticity of flow at the top of the Greater Himalayan slab, Everest, Tibet. Journal of the Geological Society (London) 161, 305–320.
Law, R.D., Morgan, S.S., Casey, M., Sylvester, A.G., Nyman, M., 1992. The Papoose Flat pluton of eastern California: a re-assessment of its emplacement history and crystallographic fabric observations. Transactions of the Royal Society of Edinburgh: Earth sciences 83, 361–375.
Law, R.D., Knipe, R.J., Dayan, H., 1984. Strain-path partitioning within thrust sheets: microstructural and petrofabric evidence from the Moine thrust zone at Loch Eriboll, northwest Scotland. Journal of Structural Geology 6, 477–497.
Lister, G.S., Snoke, A.W., 1984. S–C mylonites. Journal of Structural Geology 6, 617–663.
Lister, G.S., Dornsiepen, U.F., 1982. Fabric transitions in the Saxony granulite terrain. Journal of Structural Geology 4, 81–92.
Lister, G.S., Hobbs, B.E., 1980. The simulation of fabric development during plastic deformation and its application to quartzite: fabric transition. Journal of Structural Geology 1, 99–115.
Lo, C.H., Onstott, T.C., 1989. ^{39}Ar recoil artifacts in chloritized biotite. Geochimica et Cosmochimica Acta 53, 2697–2711.
Lovera, O.M., Grove, M., Harrison, T.M., 1989. The $^{40}Ar/^{39}Ar$ geothermometry for slowly cooled samples having a distribution of diffusion domain sizes. Journal of Geophysical Research 94, 17917–17935.
Mainprice, D., Bouchez, J.L., Blumefeld, Ph., Tubia, J.M., 1986. Dominant c-slip in naturally deformed quartz: implication for dramatic plastic softening of high temperature. Geology 14, 819–822.
Markley, M., Teyssier, C., Cosca, M., 2002. The relation between grain size and $^{40}Ar/^{39}Ar$ date for Alpine white mica from the Siviez-Mischabel Nappe, Switzerland. Journal of Structural Geology 24, 1937–1995.
McDougall, I., Harrison, T.M., 1988. Geochronology and thermochronology by the $^{40}Ar/^{39}Ar$ method. In: Oxford Monographs on Geology and Geophysics, vol. 9. University Press, Oxford.
Means, W.D., 1994. Rotational quantities in homogeneous flow and development of small-scale structures. Geology 16, 437–446.
Means, W.D., Hobbs, B.E., Lister, G.S., Williams, P.F., 1980. Vorticity and non-coaxiality in progressive deformation. Journal of Structural Geology 2, 371–378.
Nicolas, A., 1989. Structures in Ophiolites and Dynamics of Oceanic Lithosphere. Kluwer, Dordrecht, 367 pp.
Nicolas, A., Boudier, F., Ildefonse, B., Bell, E., 2000. Accretion of Oman and United Arab Emirates ophiolites – discussion of a new structural map. Marine Geophysical Researches 21, 147–179.
Nyman, M.W., Law, R.D., Morgan, S.S., 1995. Conditions of contact metamorphism, Papoose Flat Pluton, eastern California, USA: implications for cooling and strain histories. Journal of Metamorphic Geology 13, 627–643.
Okudaira, T., Takeshita, T., Hara, I., Ando, J., 1995. A new estimate of the conditions for transition from basal <a> to prism [c] slip in naturally deformed quartz. Tectonophysics 250, 31–41.
Passchier, C.W., 1998. Monoclinic model shear zones. Journal of Structural Geology 20, 1121–1137.
Passchier, C.W., 1997. The fabric attractor. Journal of Structural Geology 19, 113–127.
Passchier, C.W., 1988. Analysis of deformation paths in shear zones. Geologisches Rundschau 77, 309–318.
Passchier, C.W., Trouw, R.A.J., 2005. Microtectonics. Springer, Berlin, Heidelberg, New York.
Passchier, C.W., Urai, J.L., 1988. Vorticity and strain analysis using Mohr diagrams. Journal of Structural Geology 10, 755–763.
Passchier, C.W., 1987. Stable positions of rigid objects in non-coaxial flow: a study in vorticity analysis. Journal of Structural Geology 9, 679–690.
Passchier, C.W., Simpson, C., 1986. Porphyroclast systems as kinematic indicators. Journal of Structural Geology 8, 831–844.
Parlak, O., Delaloye, M., 1999. Precise $^{40}Ar/^{39}Ar$ ages from the metamorphic sole of the Mersin ophiolite (southern Turkey). Tectonophysics 301, 145–158.

Pickles, C.S., Kelley, S.P., Reddy, S.M., Wheeler, J., 1997. Determination of high spatial resolution argon isotope variations in metamorphic biotites. Geochimica et Cosmochimica Acta 61 (180), 3809–3883.
Platt, J.P., Behrmann, J.H., 1986. Structures and fabrics in a crustal scale shear zone, Betic Cordilleras, SE Spain. Journal of Structural Geology 8, 15–34.
Ramsay, J.G., Huber, M.I., 1987. The technique of modern structural geology. In: Folds and Fractures, vol. 2. Academic press, London.
Ramsay, J.G., 1962. Interference patterns produced by the superposition of folds of "similar" type. Journal of Geology 60, 466–481.
Ricou, L.E., 1968. Une coupe a travers les series a radiolarites des Monts Pichakun (Zagros, Iran). Bulletin for Geology 10 (Fr.7 Series), 478–485.
Sabzehei, M., Roshan Ravan, B., Eshraghi, S.A., Alai Mahabadi, S., Saraj, M., 1993. Geological Map of the Neyriz Quadrangle H-11, Scale: 1:250,000. Geological Survey of Iran, Tehran, Iran.
Sanderson, D.J., Marchini, W.R.D., 1984. Transpression. Journal of Structural Geology 6, 449–458.
Sarkarinejad, K., 2007. Quantitative finite strain and kinematic flow analyses along the Zagros transpression zone, Iran. Tectonophysics 442, 49–65.
Sarkarinejad, K., 2005. Structures and microstructures related to steady-state mantle flow in the Neyriz ophiolite, Iran. Journal of Asian Earth Sciences 25, 859–881.
Sarkarinejad, K., 2003. Structural and microstructural analysis of a palaeo-transform fault zone in the Neyriz ophiolite, Iran. In: Dilek, Y., Robinson, R.T. (Eds.), Ophiolites in Earth History. Geological Society, London, Special Publications, vol. 218, pp. 129–145.
Sarkarinejad, K., 1999. Tectonic finite strain analysis: using Ghouri deformed conglomerate, Neyriz area, southwestern Iran. Iranian Journal of Science and Technology 23, 351–363.
Sarkarinejad, K., Azizi, A., 2008. Slip partitioning and inclined dextral transpression along the Zagros Thrust System, Iran. Journal of Structural Geology 30, 116–136.
Schmid, S., Casey, M., 1986. Complete fabric analysis of some commonly observed quartz *c*-axis patterns. American Geophysical Union Geophysical Monograph 36, 263–286.
Simpson, C., De Paor, D.G., 1997. Practical analysis of general shear zones using the porphyroclast hyperbolic distribution method: an example from the Scandinavian Caledonides. In: Sengupta, S. (Ed.), Evolution of Geological Structures in Micro- to Macro- Scales. Chapman and Hall, London, pp. 169–184.
Simpson, C., De Paor, D.G., 1993. Strain and kinematic analysis in general shear zones. Journal of Structural Geology 15, 1–20.
Stock, P., 1992. A strain model for antithetic fabric rotation in shear band structure. Journal of Structural Geology 14, 1267–1275.
Stocklin, J., 1974. Possible Ancient Continental Margins in Iran: In the Geology of the Continental Margins. In: Burks, C.A., Drake, C.L. (Eds.). Springer-Verlag, New York, pp. 873–887.
Stocklin, J., 1968. Structural history and tectonics of Iran: a review. Bulletin of the American Association of Petroleum Geologists 52, 1229–1258.
Sullivan, W.A., Law, R.D., 2007. Deformation path partitioning within the transpressional White Mountain shear zone, California and Nevada. Journal of Structural Geology 29, 583–598.
Teyssier, C., Tikoff, B., 1999. Fabric stability in oblique convergence and divergence. Journal of Structural Geology 21, 969–974.
Teyssier, C., Tikoff, B., Markley, M., 1995. Oblique plate motion and continental tectonics. Geology 23, 447–450.
Tikoff, B., Teyssier, C., 1994. Strain modeling of displacement field partitioning in transpressional orogens. Journal of Structural Geology 16, 1575–1588.
Tikoff, B., Fossen, H., 1995. The limitations of three-dimensional kinematic vorticity analysis. Journal of Structural Geology 12, 1771–1784.
Tullis, J.A., Christie, J.M., Griggs, D.T., 1973. Microstructures and preferred orientations of experimentally deformed quartzites. Geological Society of America Bulletin 84, 297–314.
Turner, F.J., 1968. Metamorphic Petrology: Mineralogical and Field Aspects. McGraw-Hill, New York.
Vernant, P., Nilforoushan, F., Hatzfeld, D., Vigny, C., Masson, F., Nankal, H., Martino, J., Ashtiani, A., Baye, R., Tavakoli, F., Chery, J., 2004. Present-day crustal deformation and plate kinematics in the Middle East constrained by GPS measurements in Iran and northern Oman. International Journal of Geophysics 157, 381–398.
Vissers, R.L.M., 1989. Asymmetrical quartz *c*-axis fabrics and flow vorticity: a study using rotated garnets. Journal of Structural Geology 11, 231–244.
Wilson, J., Dallmeyer, R.D., Grocott, J., 2000. New $Ar^{40}/^{39}Ar$ dates from the Tazas complex, northern Chile: tectonic significance. Journal of South American Earth Sciences 13, 115–122.
Wilson, C.J.L., 1975. Preferred orientation in quartz ribbon mylonites. Geological Society of America Bulletin 86, 968–974.
Wallis, S.R., 1995. Vorticity analysis and recognition of ductile extension in the Sanbagawa Belt, SW Japan. Journal of Structural Geology 17, 1077–1093.
Wallis, S.R., 1992. Vorticity analysis in metachert from Sanbagawa Belt, SW Japan. Journal of Structural Geology 14, 271–280.
Wenk, H.R., 1994. Preferred orientation patterns in deformed quartzites. In: Heaney, P.J., Prewitt, C.T., Gibbs, G.V. (Eds.), Silica: Physical Behavior, Geochemistry and Material Applications. Reviews in Mineralogy, vol. 29, pp. 177–208.
York, D., Lopez Martinez, M., 1986. The two-faced mica. Geophysical Research Letters 9, 937–975.